The influence of the temperature distributions inside a TRISO-particle and fuel pin on the neutron multiplication factor

Soufyan Roubiou

Bachelor of Science Thesis

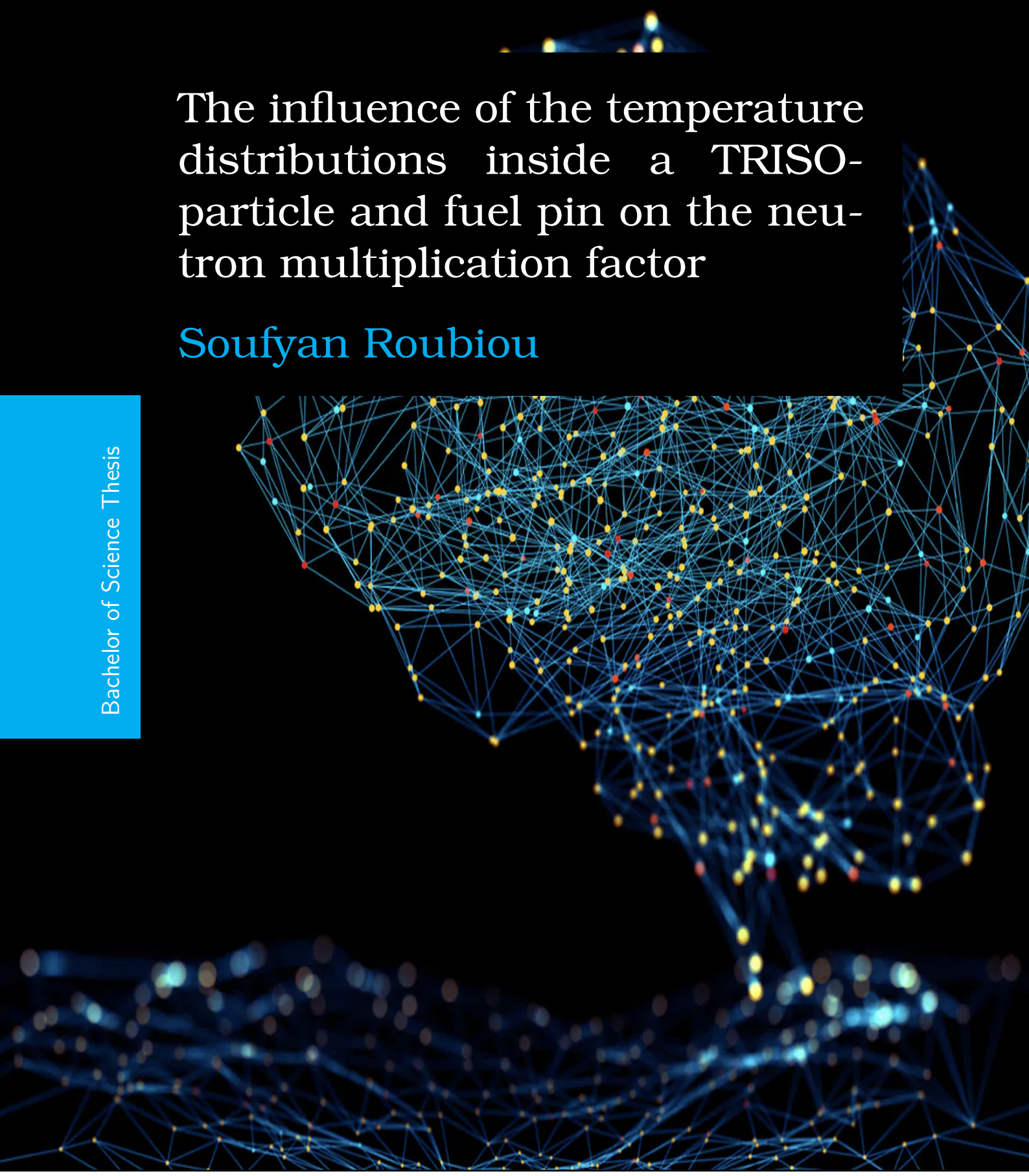

TU Delft Delft University of Technology

BSc Applied Physics

The influence of the temperature distributions inside a TRISO-particle and fuel pin on the neutron multiplication factor

Bachelor of Science Thesis

For the degree of Bachelor of Science in Bsc Applied Physics at Delft University of Technology

Soufyan Roubiou

February 16, 2022

Faculty of Applied Sciences (TNW) · Delft University of Technology

Delft University of Technology
Department of
Delft Center for Applied Sciences (dcsc)

The undersigned hereby certify that they have read and recommend to the Faculty of Applied Sciences (TNW) for acceptance a thesis entitled

The influence of the temperature distributions inside a TRISO-particle and fuel pin on the neutron multiplication factor

by

Soufyan Roubiou

in partial fulfillment of the requirements for the degree of

Bachelor of Science Bsc Applied Physics

Dated: February 16, 2022

Supervisor(s):

Dr. ir. D. Lathouwers, Drs. ir. M. Van den Berg

Reader(s):

Prof. Dr. ir. J. L. Kloosterman

Abstract

The U-battery® is a small modular reactor based on the design of the high temperature gas-cooled reactor. In this report, the U-battery® is researched in order to determine the local temperature distribution and the influence thereof on the multiplication factor k inside the reactor core and whether this is important for a future U-battery® model. The U-battery® core consists of fuel blocks containing fuel channels and cooling channels.

The temperature distribution is researched by determining the temperature distribution over a TRISO particle, over the radial plane of a fuel pin inside the reactor core and lastly over the entire core. The TRISO-particle has a maximum temperature difference of $\Delta T = 2.18K$ between its core and outer surface. The fuel pin has a maximum temperature difference of $\Delta T = 15.86$K. The temperature distributions are used to determine the Fuel Temperature Coefficient (FTC). It is found that the FTC $\alpha_f \approx -2.22$ [pcm/K].

Furthermore, the temperature distribution inside the reactor core is determined by numerically approaching the heat equation using the discontinuous Galerkin finite volume method. To do this we use a simplified model for the U-battery®. The temperature of the coolant T_c flows in at $T_{in} = 523$K and on average increases by $\Delta T \approx 475$K over the height of the reactor. The graphite temperature T_g ranges from $T = 600$K to $T = 1173$K at $r = 0$ over the height of the reactor and from $T = 564$K to $T = 866$K at $r = R_{max}$ over the height of the reactor. On average, T_g increases by $\Delta T \approx 467$K over the height of the reactor. Based on the findings of this research, it is not necessary to include local temperature variations inside the reactor core in a future model of the U-battery®.

Table of Contents

List of Figures

List of Tables

Preface & Acknowledgements

I would like to thank my supervisor Dr. D. Lathouwers for his assistance and advice during the writing of this thesis. Also, I would like to thank Marc van den Berg for his help, support and guidance during the research and writing of my thesis. Furthermore, special thanks to Prof. Dr. J.L. Kloosterman for reading my thesis and being in my committee.

Delft, University of Technology
February 16, 2022

Soufyan Roubiou

“Voor mijn Mama en Papa.”
— *Soufyan Roubiou*

Chapter 1

Introduction

1-1 Introduction

Earth's temperature has risen by 0.08° C per decade since 1880, and the rate of warming over the past 40 years is more than twice that: 0.18° C per decade since 1981. 2020 was the second-warmest year on record based on NOAA's (National Oceanic and Atmospheric Administration) temperature data, and land areas were record warm. [11] Based on predictions, this trend will only seem to continue itself, which is why the need for energy that emits less CO_2 is ever more persistent.

One of these sources is nuclear energy, which has gained renewed attention as a reliable and clean source of energy. In particular, one type of nuclear reactor has gained more attention and traction: Small Modular Reactors. As opposed to conventional nuclear reactors, SMRs are smaller, easier to transport and also safer. This makes them a viable alternative for power generation in remote areas, for example to replace diesel generators.

A design of an SMR currently under development is the U-battery®. The U-battery® is an advanced commercial SMR, which is designed to provide low-carbon, cost effective energy for energy heavy industries and remote areas. It is a high temperature gas-cooled (HTGR) reactor with a core lifetime of 5 to 10 years. [12] The conceptual design was developed by the Universities of Manchester (UK) and Delft (Netherlands) after the project was initiated in 2008. [13] Two designs were proposed, a 20MWth and a 10MWth design, in this thesis the 20MWth design is researched. The overall design parameters implemented for the 20MWth U-battery® can be found in Table 1.1.

Table 1-1: Design parameters used for the U-battery [1]

Parameter	Value
Thermal Power	20 MWth
Coolant	Helium
Moderator	Graphite
Pressure	4.0 MPa
Total mass flow coolant	7.64 kg/s
Inlet temperature	523K
Core diameter, height	252cm, 320cm
Fuel Type	UO_2, TRISO coated fuel

Although the U-battery® is an entire nuclear reactor on its own, this thesis will only focus on the core of the reactor. The core of the U-battery® consists of a fuel zone surrounded by reflectors. The fuel zone consists of fuel blocks containing fuel channels, cooling channels, and, in the final design of the U-battery®, burnable poison rods. Figure 1-1a displays the reactor core. Figure 1-1b zooms in on a fuel block, showing the different components inside of it.

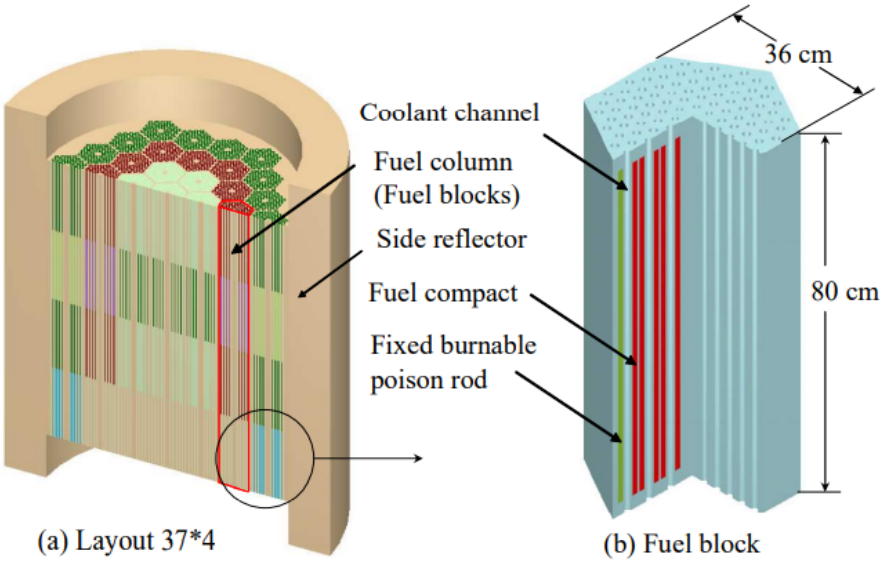

Figure 1-1: A schematic representation of the core in Figure a, containing 37x4 fuel blocks, they are stacked on top of each other and placed in a hexagonal layout, surrounded by the graphite reflector. Figure b shows a fuel block and the components inside a fuel block. [1]

Figure 1-2 shows the cross section of a fuel block, the block is 36cm wide and has a height of 80cm. It contains 216 fuel channels and 108 coolant channels, with a diameter of 1.27cm and 1.588cm respectively. The inner 6 coolant channels have a diameter of 1.27cm. [1] The coolant channels are filled with helium that is pumped through the channels under high pressure (see Table 1). The fuel channels contain the nuclear fuel, in the case of the U-battery®, TRISO fuel is used. The rest of the fuel block is filled with graphite, which acts as a moderator. The

function of the moderator will further be explained in chapter 2.

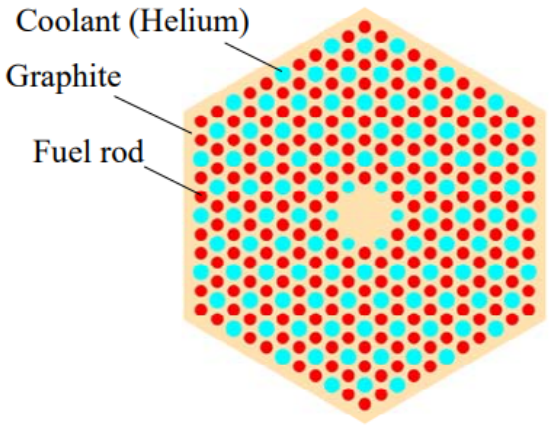

Figure 1-2: The cross section of a fuel block. The blue dots are cooling channels with a diameter of 1.588cm, except for the inner 6 cooling channels, which have a diameter of 1.27cm. The red dots are fuel rods with a diameter of 1.27cm. [1]

The fuel type used in the U-battery® is tri-structural isotropic (TRISO) coated fuel, this is a fuel type containing UO_2 in its kernel, encapsulated by three layers of carbon- and ceramic-based materials that prevent the release of radioactive fission products.[14]. A schematic representation of a TRISO-particle is seen in Figure 1-3.

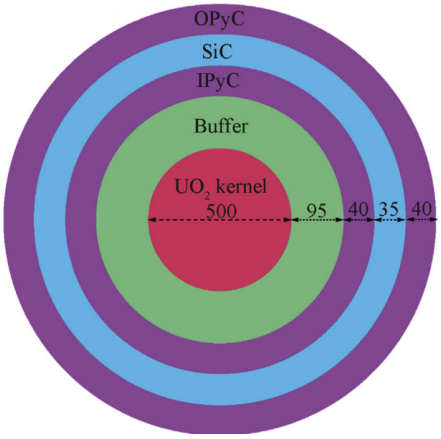

Figure 1-3: A schematic representation of a TRISO-particle, visualizing the UO_2 kernel, its surrounding protective layers and respective radii and thickness in micrometers. [2]

Here the buffer layer is a porous carbon buffer layer and is followed in sequence by an inner pyrolytic carbon (IPyC) layer, a silicon carbide (SiC) layer, and an outer pyrolytic carbon (OPyC) layer [15]. TRISO fuels are structurally more resistant than traditional reactor fuels to neutron irradiation, corrosion, oxidation and high temperatures up to 1600°C, all of which can impact fuel performance [14]. Due to their proven track record, they are also the fuel of choice in the U-battery. The TRISO particles are compacted in cylindrical fuel pellets mixed with graphite, which are then stacked in the fuel rods.

For this thesis, the effect of temperature on the fuel performance is especially important. A key component of a nuclear reactor is that a nuclear reaction sustains itself as a chain reaction once it starts. The rate at which this reaction rate happens, is called the fission rate. The fission rate can be influenced by the neutron multiplication factor k. Furthermore, the speed at which the fission rate changes is influenced by k.

In this thesis the influence of temperature differences throughout the reactor core on the neutron multiplication factor is researched. More specifically, the temperature distribution of a TRISO-particle, a fuel pin and the reactor core itself will be determined. This is done to research whether these temperature differences have an effect on k, and whether this effect is significant enough to take into consideration for a future U-battery® model. This will be done by deriving a thermal-hydraulic model for the core of the reactor using the discontinuous Galerkin finite volume method.

The thesis is organised as follows: chapter 2 covers the analytical models used in the study; it covers theory regarding the neutron multiplication factor and the influence of temperature and other variables on k; furthermore it covers the derivation of the temperature distribution inside a TRISO-particle and a fuel pin and the methods used to solve the analytical models. Subsequently chapter 3 covers the numerical model used in the study; we derive the temperature distribution for the core of the reactor and how to numerically approach it with the discontinuous Galerkin finite volume method and how it is used to numerically approach the temperature distribution. In chapter 4, the obtained results will be presented and discussed and finally, in chapter 5 a conclusion will be drawn and recommendations will be given.

Chapter 2

Analytical models

In this chapter the theory needed to derive temperature distributions for a TRISO-particle and a fuel pin are discussed; the temperature distributions themselves are derived and the methodology to solve the equations is discussed. The theory section is divided into two parts: the neutronics and the thermohydraulics of the U-battery®. First, the neutronics is covered in order to portray how the nuclear processes in the U-battery® work. Secondly, the thermalhydraulics will be covered. The equations needed for the temperature distribution of a TRISO-particle and a fuel pin will be derived. They are derived to research the effect they have on k.

2-1 Neutronics

2-1-1 Cross-sections

In a nuclear reactor, nuclear fission takes place. Nuclear fission is a neutron-driven chain reaction releasing energy. Two types of neutrons are released from the fission that ensues: prompt neutrons and delayed neutrons. Due to their higher importance for maintaining fission, the focus of this section will remain on prompt neutrons. A neutron is fired at a fissile particle, usually ^{235}U, which almost immediately undergoes γ-decay and sends out prompt neutrons, all within $\sim 10^{-14}$ seconds. Figure 2-1 shows a plot of the numbers of neutrons versus numbers of protons for the most stable combinations of neutrons and protons.

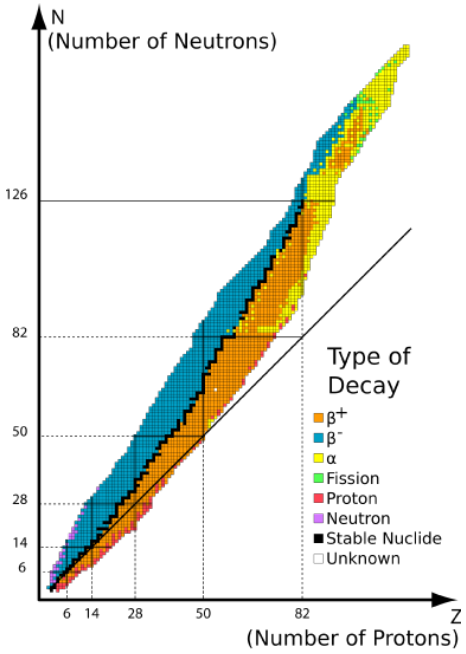

Figure 2-1: Relation between the number of protons and neutrons, highlighting the most stable combinations [3]

The amount of neutrons the fission products emit, depend on the incident energy of the neutrons. This relation is depicted in Figure 2-2.

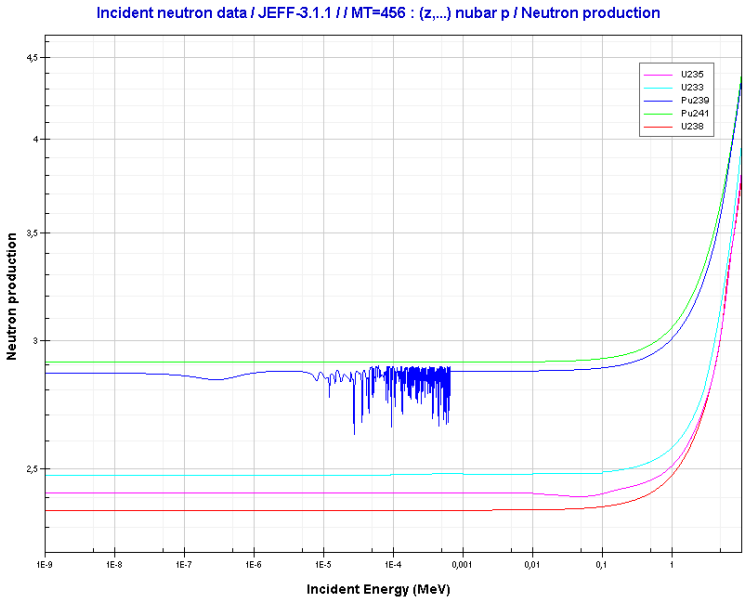

Figure 2-2: Logarithmic plot of the relation between neutron production and incident neutron energy (MeV) for several radioactive isotopes. In this thesis ^{235}U will be used as an example, as it is the fissile isotope being used in the U-battery®[4].

Looking at the relation for ^{235}U, the neutron production is near constant for lower incident energies. As incident energy increases, neutron production rate increases too due to the fact that the target nucleus gains energy too and therefore may undergo different nuclear reactions. Since the U-battery® is a thermal reactor, it is preferable to create thermal neutrons to increase the chance of fission. Thermal energies are usually energies below 1 eV.

A way to visualize this is by the use of neutron cross-sections. This is an effective area that quantifies the likelihood of a certain interaction of an incident neutron with a given target nucleus [7]. One type of cross-sections is the microscopic cross-section. Microscopic cross-sections define the 'effective target area' of a single nucleus to an incident neutron beam. The larger this effective target area is, the greater the probability is for a reaction. An example of a fission cross section for ^{235}U is shown in Figure 2-3.

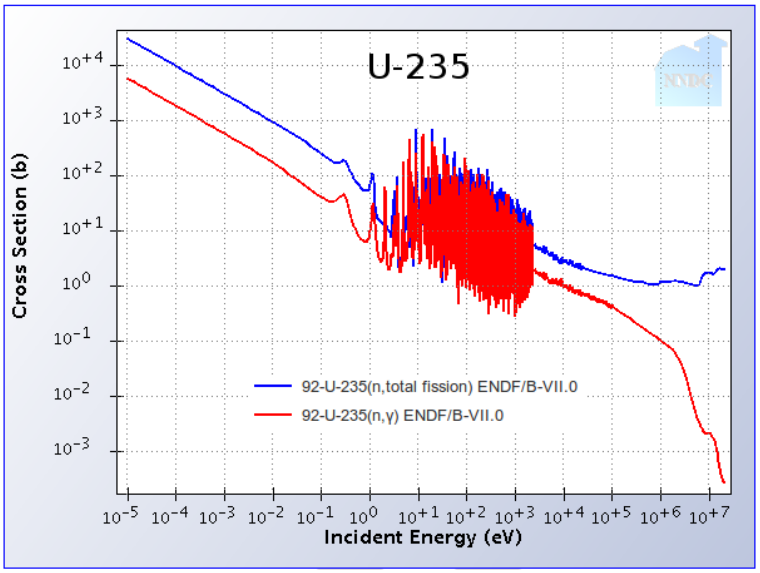

Figure 2-3: Fission cross section of ^{235}U. The cross section increases as the incident energy decreases, meaning more fission takes place for these energies. [4]

Figure 2-3 shows that at high incident energies, the probability of fission is relatively low compared to the probability of fission for low incident energies. It follows that almost all of the fission in thermal reactors happens at the lower (thermal) energies, which ties back to Figure 2-2 and what was mentioned before. The oscillations in the middle of the plot is called the resonance region. When a neutron beam hits a target nucleus, the ensuing nuclear reaction sometimes only takes place when the energy of the compound nucleus is in the neighborhood of so called resonance energies, explaining why only some energies have an increase in cross-section in the resonance region. This is due to discretized energy levels. [7] The probability of absorption also increases, which will further be explained in section 2.1.2.

The resonance region of a cross-section is dependent on the fuel temperature due to the effect of Doppler broadening. In general, the target nuclei have a thermal energy, which causes them to vibrate in their lattice structure. Due to this back and forth vibration, incident neutrons appear to have a continuous distribution of kinetic energies. As fuel temperature increases, the thermal energy of the target nuclei increases. Due to the increased thermal energy, the target nuclei vibrate faster in their lattice structure. This in turn causes the compound nucleus to have a wider distribution of energies for one incident neutron energy, effectively shortening and widening the energy distribution of the compound nucleus as depicted in Figure 2-4.

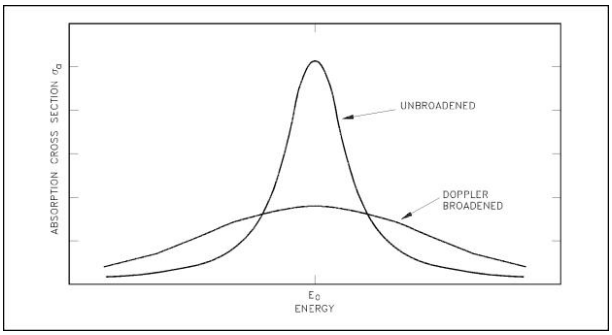

Figure 2-4: Visualization of Doppler broadening on a resonance peak. The resonance peak becomes shorter and wider due to the fact that the neutron appears to have a broadened energy distribution, owing to the increased vibrations of the target nuclei. [5]

2-1-2 Neutron multiplication factor

To understand the effect of Doppler broadening, the (effective) neutron multiplication factor k_{eff} is introduced. The goal of a nuclear reactor is to have a stable, self-sustained fission reaction. This implies that for every neutron absorbed or otherwise lost in a fission reaction, on average at least one neutron should be produced by the fission reaction in question.

k_{eff} describes this condition as the ratio between neutrons produced from fission in one generation divided by the neutrons lost (due to absorption, leakage, etc.) in the preceding neutron generation[16]. This can lead to three situations: $k_{eff} < 1$, $k_{eff} > 1$ and $k_{eff} = 1$. Nuclear reactors strive to have $k_{eff} = 1$, as it implies that for every neutron used in a fission process, it on average produces exactly one neutron over time. The neutron population remains constant and the fission process is self-sustaining. This is known as the critical state.

One important nuclear process that influences k_{eff} is the resonance escape probability. Figure 2-5 shows the fission neutron energy distribution for thermal fission of ^{235}U [6]. The average neutron energy is about 2 MeV [17]. As has been noted in Figure 2-3, the fission probability increases as the incident neutron energy decreases. To be able to do this, most nuclear reactors use a moderator material to slow down these neutrons. Typical moderator materials are hydrogen and carbon. The U-battery® uses graphite as its moderator.

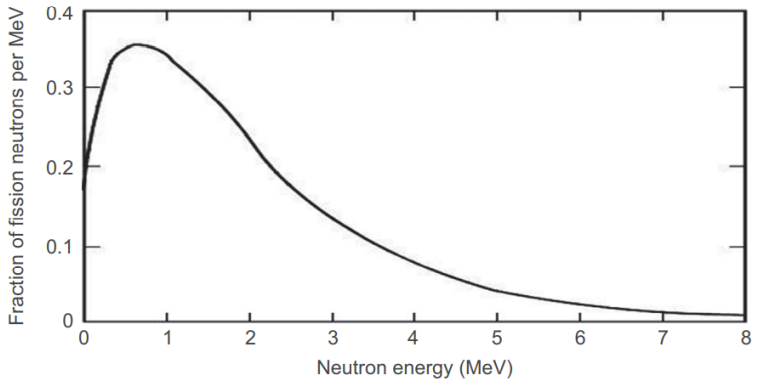

Figure 2-5: Fission neutron energy spectrum for thermal fission of ^{235}U [6].

The moderator slows these fast neutrons down to a thermal energy [17]. However, during this thermalization, neutrons may not only collide with moderator nuclei, but also with fuel nuclei. It is possible that neutrons may carry an energy in the resonance region, resulting in the possibility of these neutrons being captured. The probability that a neutron will not be captured in the entire resonance region is called the resonance escape probability. The probability is defined as the number of neutrons that reach thermal energies divided by the number of fast neutrons that are slowed down initially [16].

The factors that affect the resonance capture probability the most are changes in the moderator and fuel temperature. Most reactors are so-called under moderated. As the moderator-to-fuel ratio increases, Figure 2-6 shows that an under-moderated reactor will have higher resonance absorption. This is due to the fact that the neutrons will now stay at a higher energy for a longer period of time, thus increasing the probability of these neutrons colliding with the target nuclei and being absorbed in the resonance region [7].

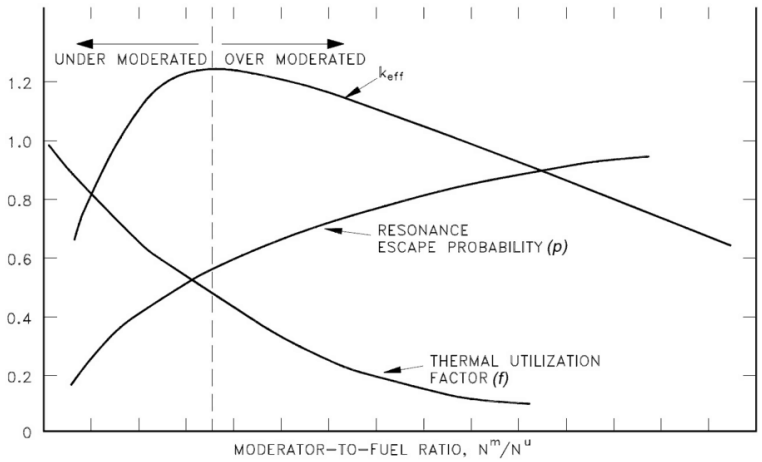

Figure 2-6: Plot of the resonance escape probability, thermal utilization factor and under- and over-moderation of the core as a function of the moderator-to-fuel ratio. The y-axis is k_{eff}. [7]

For the U-battery® specifically, the change in fuel temperature is significant. This is connected with Doppler broadening due to the broadening of the resonance peaks, resulting in more neutrons being captured and the resonance capture probability decreasing, and thus in turn decreasing k_{eff}. Changes in k_{eff} are described by the reactivity ρ_r, which is defined as

$$\rho_r = \frac{k_{eff} - 1}{k_{eff}}. \tag{2-1}$$

It is then useful to define the change in reactivity per degree change in fuel temperature,

$$\alpha_f = \frac{d\rho_r}{dT_f} = \frac{1}{k_{eff}^2} \frac{\partial k_{eff}}{\partial T_f}, \tag{2-2}$$

which is called the Fuel Temperature Coefficient (FTC) or Doppler Temperature Coefficient (DTC). It is expressed in units of [pcm/°C] or [pcm/K], with pcm (per cent mille) being 1/1000th of a percent of the reactivity. Doppler broadening of resonances is important because it accounts for the dominant part of the FTC. The FTC should be negative at all temperatures, and therefore provides an important negative feedback in case of inserted positive reactivity [7]. Furthermore, previous research by Ding has shown that the U-battery® has a negative FTC during its whole lifetime [12]. The time for the FTC to take into effect is almost instantaneous, providing immediate negative reactivity in case of inserted positive reactivity, thus ensuring reactor stability.

In this thesis, the effect of changes in the fuel temperature on the reactivity due to (mainly) Doppler broadening will be researched. In order to do that, the governing temperature equations for different components in the reactor core will be subsequently determined in the rest of chapter 2.

2-2 Fourier's law

2-2-1 Fourier's law in spherical coordinates

A temperature difference can be a driving force behind the transfer of internal (heat) energy by particles colliding with each other. This heat transfer, or heat flow, is indicated by ϕ_q [W]. The heat flux, ϕ_q'' $[\frac{W}{m^2}]$, is then defined as the heat flow perpendicular through a surface area A $[m^2]$, and is given as $\phi_q'' = \frac{\phi_q}{A}$.

To be able to describe heat conduction in spherical coordinates, we assume a sphere of radius R with temperature $T(r)$ and constant thermal conductivity λ in a material with temperature T_f far away from the sphere. To determine the heat conduction equation, we look at a small part of the sphere, with radii r and $r + dr$, we can write the heat balance, assuming steady-state conditions, as:

$$\frac{dU}{dt} = 0 = \phi_{q,in} - \phi_{q,out}, \tag{2-3}$$

where U is the total internal energy. $\phi_q^{''}$ can be expressed in terms of the gradient in the temperature by Fourier's law. This law states that the time rate of heat transfer per unit area through a material is proportional to the negative gradient in the temperature [18]:

$$\phi_q^{''}(r) = -\lambda \frac{dT(r)}{dr}, \tag{2-4}$$

where λ is the materials thermal conductivity $[\frac{W}{mK}]$. The surface area of a sphere is dependent on r via $A(r) = 4\pi r^2$. In the case of a fissile particle with radius R, surface temperature T_s and uniform heat production over its volume, the heat balance gains an additional term, the volumetric power density $q_f^{'''}$ [W/m^3] by fission. The heat balance over a small part of the sphere $[r, r + dr]$ then reads

$$0 = -\lambda \cdot A(r) \frac{dT(r)}{dr}\bigg|_r - \left(-\lambda \cdot A(r) \frac{dT(r)}{dr}\bigg|_{r+dr} \right) + q_f^{'''} 4\pi r^2 dr. \tag{2-5}$$

We can simplify this using the following relation:

$$f(x + dx) = f(x) + \frac{df}{dx} \cdot dx, \tag{2-6}$$

Equation 2-5 then simplifies to

$$\frac{d}{dr}\left(r^2 \frac{dT(r)}{dr} \right) = \frac{q_f^{'''} r^2}{\lambda}. \tag{2-7}$$

Integrating this equation gives

$$r^2 \frac{dT(r)}{dr} = -\frac{q_f^{'''} r^3}{3\lambda} + C_1. \tag{2-8}$$

Since the temperature is maximal, and therefore the derivative $\dfrac{dT(r)}{dr} = 0$ at $r = 0$, $C_1 = 0$ must hold. It follows that, given the boundary condition $T = T_s$ at $r = R$, the equation for the temperature of a radioactive particle can be given as

$$T(r) = T_s + \frac{q_f^{'''}}{6\lambda}(R^2 - r^2). \tag{2-9}$$

Setting $r = 0$ will give the temperature in the core of the particle.

2-2-2 Applying Fourier's Law to TRISO-particles

TRISO-particles have, next to a heat producing core, multiple layers surrounding the cores. To determine the heat conduction through these layers, a heat balance can be used in combination with the heat flux through these surfaces. Since these layers are already spherical shells, it is not necessary to consider a small shell $[r,\ r + dr]$. Instead, we can immediately derive

the formula for the temperature from the heat flux through its surface area. We know that $\phi_q = A(r)\phi_q''(r)$, where ϕ_q is the heat flow from the core to the surrounding layers. It is constant for every layer, but the heat flux differs for every layer, as it is dependent on $A(r)$. By applying this to Equation 2-4 we get

$$\frac{dT(r)}{dr} = -\frac{\phi_q}{4\pi r^2 \lambda_i} \tag{2-10}$$

for the layers surrounding the core, so in other words, for $r > R_1$, where R_1 is the radius of the heat producing core. Furthermore, λ_i is the heat conduction coefficient for the respective layers. We can integrate this equation and apply a boundary condition for the integration constant C_1. For the outer radius, R_6, we (for now) assume a temperature $T_6 = 800K$. Solving this for C_1 we find that

$$T(r) = 800 + \frac{\phi_q}{4\pi\lambda_i}\left(\frac{1}{r} + \frac{1}{R_6}\right) \tag{2-11}$$

for the outer spherical shell, in other words, for $R5 < r < R6$. This equation can then recursively be used to find the temperature of all spherical shells up to the core. This is done in Python using the values displayed in Table 2.1 for the heat conductivities and radii of the TRISO-particle.

Table 2-1: Initial values used for the heat conductivities and radii of the TRISO-particle to determine the core temperature [2]

material	$\lambda(W/cmK)$	$r(\mu m)$
UO_2 kernel	0.0386	250.0
Buffer	0.005	345.0
IPyC	0.04	385.0
SiC	0.1	420.0
OPyC	0.04	460.0
Graphite	0.25	1000.0

2-2-3 Fourier's law in cylindrical coordinates

In order to determine the temperature distribution inside a fuel pin in the reactor core, Fourier's law in cylindrical coordinates is needed. Assume a heat producing cylinder with a volumetric power density q_f''' surrounded by a conducting cylindrical shell, where the heat producing cylinder ranges from $0 < r < R_1$, and the cylindrical shell from $R_1 < r < R_2$, and at R_1 $T = T_1$. For the remainder of the calculations, we assume the length of the cylinder is sufficiently large. We can then look at a small strip with radii r and $r + dr$ inside the core and derive a heat balance for this strip, assuming steady state and uniform heat production, it follows that

$$0 = -2\pi r L \cdot \lambda \frac{dT}{dr}\bigg|_r - \left(- \lambda 2\pi r L \frac{dT}{dr}\bigg|_{r+dr}\right) + q_f''' 2\pi r L dr, \tag{2-12}$$

where the area $A(r) = 2\pi rL$. Using Equation 2-6, Equation 2-12 simplifies to:

$$\frac{d}{dr}\left(r\frac{dT}{dr}\right) = -\frac{q'''_f r}{\lambda}. \tag{2-13}$$

Integrating once and applying the boundary condition $\frac{dT}{dr} = 0$ at $r = 0$, gives us

$$\frac{dT}{dr} = -\frac{q'''_f r}{2\lambda}. \tag{2-14}$$

Intergrating again with the boundary condition $T = T_1$ at $r = R_1$ gives us the final equation for the massive cylinder:

$$T(r) = T_1 + \frac{q'''_f}{4\lambda}(R_1^2 - r^2). \tag{2-15}$$

For the cylindrical shell around it, we know that $\phi_q = A(r)\phi''_q$, which we can rewrite using Fourier's law to

$$\frac{dT}{dr} = -\frac{\phi_q}{2\pi rL\lambda_i}, \tag{2-16}$$

where λ_i is again the thermal conductivity for each respective layer. Integrating this gives

$$T(r) = -\frac{\phi_q ln(r)}{2\pi L\lambda_i} + C_1. \tag{2-17}$$

Applying the second boundary condition, $T = T_2$ at $r = R_2$, and solving for C_1 and plugging back into the equation gives us

$$T(r) = T_2 + \frac{\phi_q ln(\frac{R_2}{r})}{2\pi L\lambda_i}. \tag{2-18}$$

In the case of a fuel pin in the reactor core, with varying volumetric power densities, Equation 2.13 can still be used. Integrating twice gives

$$T(r) = -\frac{q'''_{f,i} r^2}{4\lambda_i} + C_1 ln(r) + C_2. \tag{2-19}$$

However, the previous boundary conditions cannot be applied, if one wants to determine the temperature distribution at any point inside the fuel pin. This is due to the fact that the TRISO-particle density inside the fuel pin is a function of the radius r, and therefore small strips $[r, r + \Delta r]$ need to be considered. We can break down the fuel pin as a cilinder with a heat producing center and surrounding heat producing layers, where the boundaries of each layer are appropriately determined depending on the TRISO-particle density in the respective layers. Therefore $q'''_{f,i}$ was introduced in Equation 2-19, which is the volumetric power density

for the center or one of the layers, depending on the position inside the fuel pin.

For the center, Equation 2-15 can still be applied, as $\frac{dT}{dr} = 0$ at $r = 0$ still holds. To determine the temperature inside the closest shell $R_1 < r < R_2$, we realize that the temperature inside the shell depends on three factors: the incoming heat from the previous layer, in this case the core, the temperature at the outer layer of the shell, in this case $T(R_2) = T_2$ and the heat production of the shell itself. The incoming heat flow and $T(R_2) = T_2$ can be considered the only contributing factors to the temperature at $r = R_1$, applying this to Fourier's law gives

$$\left[\frac{dT}{dr}\right]_{r=R_1} = -\frac{\phi_q}{2\pi r L \lambda_2}. \tag{2-20}$$

Differentiating Equation 2-19 and plugging in Equation 2-20 at $r = R_1$ gives us

$$\frac{dT}{dr} = -\frac{q'''_{f,2} R_1}{2\lambda_2} + \frac{C_1}{R_1} = -\frac{\phi_q}{2\pi R_1 L \lambda_2}. \tag{2-21}$$

Solving for C_1 gives and plugging back into Equation 2-19 gives

$$T(r) = -\frac{q'''_{f,2} r^2}{4\lambda_2} + \left(\frac{-\phi_q}{2\pi L \lambda_2} + \frac{q'''_{f,2} R_1^2}{2\lambda_2}\right) ln(r) + C_2. \tag{2-22}$$

Then applying the second boundary condition we get

$$T_2 = -\frac{q'''_{f,2} R_2^2}{4\lambda_2} + \left(\frac{-\phi_q}{2\pi L \lambda_2} + \frac{q'''_{f,2} R_1^2}{2\lambda_2}\right) ln(R_2) + C_2. \tag{2-23}$$

The final equation for the shell surrounding the center can then be determined. This equation can also be applied to all the other surrounding shells, as the same principle and respective boundary conditions apply, generally

$$T(r) = T_i + \frac{q'''_{f,i}}{4\lambda_i}(R_i^2 - r^2) + \left(-\frac{\phi_q}{2\pi L \lambda_i} + \frac{q'''_{f,i} R_{i-1}^2}{2\lambda_i}\right) ln(\frac{r}{R_i}). \tag{2-24}$$

Where λ_i is the average thermal conductivity (which will be noted as effective thermal conductivity $\lambda_{e,i}$ from now on) in the respective shells, where each shell has a radius $R_{i-1} < r < R_i$. $\lambda_{e,i}$ depends on the so-called packing fraction of TRISO-particles inside the shell as the TRISO's have a different thermal conductivity than the graphite (see Table 2-1). A packing fraction of 0.3 would imply that 30% of the volume in question consists of TRISO-particles.

$\lambda_{e,i}$ is determined by applying the best fitting parameters by Gonzo [19] to the Chiew & Glandt model [20]:

$$\lambda_e = \lambda_m \left[\frac{1 + 2\beta\phi + (2\beta^3 - 0.1\beta)\phi^2 + \phi^3 0.05 e^{4.5\beta}}{1 - \beta\phi}\right], \tag{2-25}$$

where it is useful to introduce the ratio of the thermal conductivity of the particles to the surrounding graphite matrix [21]

$$\kappa = \frac{\lambda_p}{\lambda_m}. \tag{2-26}$$

Here λ_p is the average thermal conductivity of a TRISO-particle and λ_m is the thermal conductivity of the matrix. Furthermore, β is defined as [21]

$$\beta = \frac{\kappa - 1}{\kappa + 2}. \tag{2-27}$$

In order to apply the Chiew & Glandt model, the effective thermal conductivity of a single TRISO-particle, ETC_p (analog to the average of λ_p) needs to be determined. Stainsby et al.[22] derived this value to be 4.13 W m^{-1} K^{-1} for the values in Table 2.2. With this, everything is determined in order to derive the temperature distribution for a fuel pin inside the reactor core.

2-3 Methodology

In this section the numerical methods used to calculate the equations derived are given. The governing equation for the temperature distribution inside a fuel pin is given by Equation 2-24. Important variables here are $\lambda_{e,i}$ and $q_{f,i}$. As the TRISO-particles are not equally distributed throughout the volume of the pin, these are not constants. Figure 2-7 displays the distribution of TRISO-particles inside a fuel pin, and, more importantly, the distribution of the fission energy inside a fuel pin (which is of course dependent on the distribution of the TRISO's). This has been determined using Serpent [8].

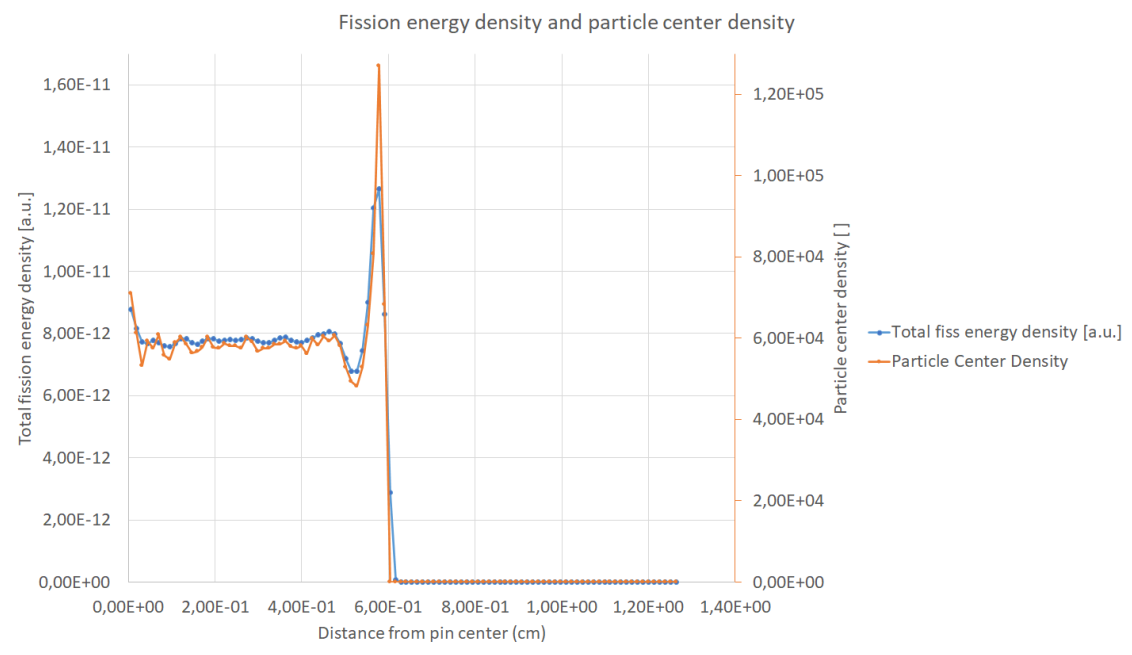

Figure 2-7: Distribution of the TRISO-particles inside a fuel pin. On the x-axis, the distance to the center of the fuel pin is displayed while the y-axis is in arbitrary units. Also shown is the distribution of the fission power inside a fuel pin [8].

The distributions in Figure 2-7 have been used to determine the volumetric power densities for every shell inside a fuel pin. This is however a simplification, as the distribution should be a continuous function of r, whereas the distributions in Figure 2-7 are discretized. The radii of the shells have been appropriately determined based on the calculated distributions. The particle distribution has also been used to calculate the average packing fraction per shell, enabling the use of Equation 2.25 for determining $\lambda_{e,i}$ in every shell. The results are displayed in chapter 4.

The resulting temperatures can be used as input for a Serpent script written to determine k_{eff}. The geometry of a fuel block is displayed in Figure 1-2. The fuel block geometry can be approximated by assuming that it contains the same components many times over. The smallest repetitive geometry is called a unit cell. The unit cell of the fuel block is determined and reflective (infinite) boundaries are assumed. A cross section of the unit cell used is displayed in Figure 2-8.

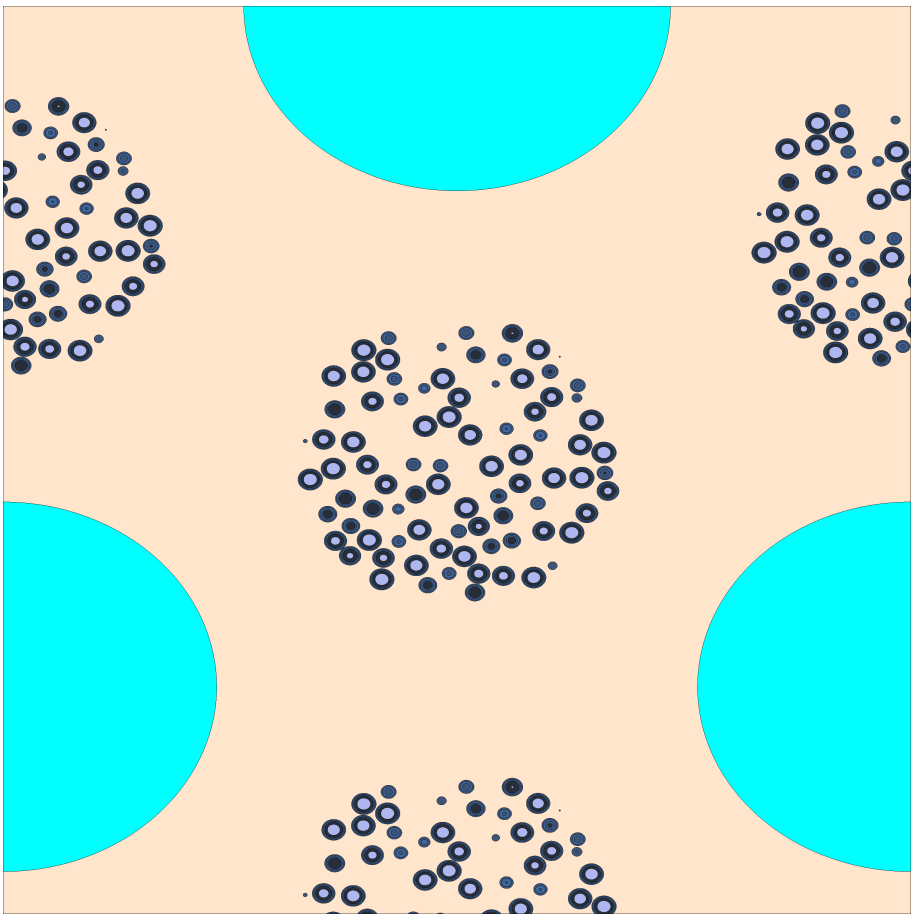

Figure 2-8: Geometry used in the Serpent simulations. Depicted is the cross section of a unit cell of the fuel block. The blue circles are cooling channels, and the collections of spheres are fuel pins containing TRISO-particles [8].

Chapter 3

Numerical Model

In this chapter, the equations needed to determine the temperature distribution inside the reactor core are determined. Furthermore, the discontinuous Galerkin finite volume method is introduced and used to numerically approach the equations for the temperature distribution. Lastly, the methodology on how to do so is covered.

3-1 Core temperature distribution

In this section, the temperature distribution of graphite T_g in the core will be determined. To this end, the distribution of the volumetric power density in the core will be approximated and the temperature distribution of the coolant will be calculated. An equation for T_g will then be derived and numerically approximated using the discontinuous Galerkin finite volume method.

3-1-1 Coolant temperature distribution

To determine the temperature distribution of the reactor core, one would need to take into account the temperature distribution of all the cooling channels and their influence upon the graphite, dependent on the geometry and location of the cooling channels. To simplify this problem, a homogeneous core is assumed, where the coolant is homogenized over the entire reactor core. The coolant flows in from the top of the core and only flows in the downward z-direction. Furthermore we assume an inlet temperature T_{in} of 523 K. Lastly, the core will be modelled as a homogenized cylinder assuming isolated boundary conditions.

Another important factor is the power distribution of the core. Depending on how this behaves as function of (r,z), it could greatly influence the temperature distribution of the reactor core. In this report it is approximated that the power distribution follows a cosine distribution in

both the r- and z-direction, where the boundaries of the core have a value of 0.5, and the center of the core has a maximum value of 1. This implies that the power distribution is largest in the center of the reactor core, and decreases as a cosine over r and z. The general equation for the volumetric power density of the core then reads

$$q_f'''(r,z) = C\cos(\alpha(z-160))\cos(\beta r), \tag{3-1}$$

where α [cm^{-1}] and β [cm^{-1}] are determined by realizing that at the outer edges of the core, the values of the cosines need to be equal to 0.5. In other words, it should hold that $\cos(\alpha(320-160)) = 0.5$ and $\cos(126\beta) = 0.5$. It follows that $\alpha = 6.54 \cdot 10^{-3} cm^{-1}$ and $\beta = 8.31 \cdot 10^{-3}$ cm^{-1}. C is the normalization factor needed to determine the right power density throughout the core. This is done by integrating $q_f'''(r,z)$ over the volume of the core and setting it equal to the power output of the core, which is 20 MWth. It follows that $C = 1.73$ W/cm^3.

To now determine the governing equation for the coolant temperature, a small ring with height $[z, z+dz]$ and radius $[r, r+dr]$ is considered. The coolant has a mass flow $\phi_{m,tot}$ over the entire surface of the core, which is equal to πR_{max}^2. It then follows that, once the cooling channels and the coolant are homogenized over the core, the mass flow ϕ_m is a function of r, and is equal to $\frac{\phi_{m,tot}}{\pi r_{max}^2} 2\pi r dr$. Furthermore, the coolant has a heat capacity c_p [J/kgK]. The energy balance over the small volume then reads

$$\frac{\phi_{m,tot}}{\pi r_{max}^2} 2\pi r dr c_p [T_c(r, z+dz) - T_c(r,z)] = \phi_{q,in}. \tag{3-2}$$

Here $\phi_{q,in}$ is the heat flow coming in from the surrounding graphite. It is assumed here that there is no conduction through the graphite, but only convection with helium. In other words, $\lambda_g = 0$. Under this assumption it follows that $\phi_{q,in}$ equals q_f''' multiplied by the small volume being considered, $2\pi r dr dz$. The energy balance then reads

$$\frac{\phi_{m,tot}}{\pi r_{max}^2} 2\pi r dr c_p [T_c(r, z+dz) - T_c(r,z)] = C\cos(\alpha(z-160))\cos(\beta r) 2\pi r dr dz. \tag{3-3}$$

Simplifying the equation and applying Equation 2-6 gives

$$\frac{\partial T_c(r,z)}{\partial z} = \frac{C\pi r_{max}^2}{\phi_{m,tot} c_p} \cos(\alpha(z-160))\cos(\beta r). \tag{3-4}$$

Integrating Equation 3-4 gives

$$T_c(r,z) = C_1 - \frac{C\pi r_{max}^2}{\phi_{m,tot} c_p \alpha} \sin(\alpha(160-z))\cos(\beta r) \tag{3-5}$$

where C_1 is an integration constant. This integration constant is found by applying the boundary condition $T(r,0) = T_{in} = 523K$. Solving this for C_1 and plugging back into the Equation leads to the final equation for $T_c(r,z)$:

$$T_c(r,z) = 523 + \frac{C\pi r_{max}^2}{\phi_{m,tot} c_p \alpha} \cos(\beta r) \Big[sin(160\alpha) - sin(\alpha(160 - z)) \Big]. \tag{3-6}$$

3-1-2 Graphite temperature distribution

Having determined the coolant temperature as a function of r and z, the heat equation in cylindrical coordinates can now be used to determine the graphite temperature. Due to the approximate angular symmetry of the problem, the angle ϕ is left out. Then $dT/d\phi = 0$ at any point inside the core. The equation then simplifies to

$$\frac{1}{r}\frac{\partial}{\partial r}\left(\lambda r \frac{\partial T_g(r,z)}{\partial r}\right) + \frac{\partial}{\partial z}\left(\lambda \frac{\partial T_g(r,z)}{\partial z}\right) = -q'''_{total}(r,z). \tag{3-7}$$

The total volumetric power density $q'''_{total}(r,z)$ is equal to the fission power density in the core minus the power absorbed by the coolant: $q'''_{total}(r,z) = q'''_f(r,z) - q'''_c(r,z)$. The first term is determined using Equation 3-1. The second term can be determined by applying Newton's law of cooling:

$$\phi_q = hA\Delta T, \tag{3-8}$$

where h is the heat transfer coefficient [W/cm^{2}K]. h is dependent on whether the flow in the core is laminar or turbulent. Table 3.1 contains relevant properties to determine the flow and h of helium. The Reynolds number is 4000 in the given temperature range, implying that the flow is turbulent. When the flow is turbulent, the coolant undergoes enough mixing to assume that the temperature difference inside a coolant channel can be disregarded. For $3000 < Re < 5000000$, the Gnielinski Equation can be used to determine the Nusselt number in tubes: [23]

$$Nu = \frac{\frac{f_D}{8}(Re - 1000)Pr}{1 + 12.7\sqrt{\frac{f_D}{8}}(Pr^{2/3} - 1)}. \tag{3-9}$$

Here f_D is the Darcy friction factor, which can be calculated using the Koo correlation[24]:

$$f_D = 4(0.0014 + 0.125Re^{-0.32}). \tag{3-10}$$

Table 3-1: Relevant properties of the coolant helium to determine the flow and the heat transfer coefficient of helium. All calculations are based on $T_{in} = 523K$ and $T_{out} = 1023K$ [10]

parameter	value at T_{in}	value at T_{out}	units	meaning
ρ	$3.7 \cdot 10^{-6}$	$1.9 \cdot 10^{-6}$	kg/cm^3	Helium density
c_p	$5.195 \cdot 10^3$	$5.195 \cdot 10^3$	J/kg/K	Helium specific heat capacity
μ	$3.04 \cdot 10^{-7}$	$4.78 \cdot 10^{-7}$	kg/cm/s	Helium dynamic viscosity
v	324	631	cm/s	Flow velocity
λ	0.0023	0.0037	W/ cm K	Helium thermal conductivity
Re	6448	4023	-	Reynolds number
Pr	0.70	0.70	-	Prandtl number
f_D	0.036	0.041	-	Darcy friction factor
Nu	21	13	-	Nusselt number
h	0.0030	0.0031	W/cm^2K	Heat transfer coefficient

It follows that the heat transfer coefficient is near constant over the given temperature interval, and will be treated and used as such in this thesis. It was mentioned that, instead of separate cooling channels, a homogeneous core is assumed to simplify the problem posed in this chapter. Because of this, it is convenient to work with the average area of cooling channel per cubic meter inside the core, noted by α [cm^{-1}]. The temperature difference in Equation 3-8 for this situation is equal to the temperature difference between the graphite and the coolant, where both depend on their position inside the core. Plugging this all into Equation 3-8 gives

$$q_c'''(r,z) = h\alpha(T_g(r,z) - T_c(r,z)), \tag{3-11}$$

where instead of the heat flow ϕ_q, the equation now determines the volumetric power density $q_c'''(r,z)$. The total volumetric power density is therefore equal to

$$q_{total}'''(r,z) = q_f'''(r,z) - h\alpha(T_g(r,z) - T_c(r,z)) \tag{3-12}$$

and plugging Equation 3-12 into Equation 3-7, it follows that

$$\frac{1}{r}\frac{\partial}{\partial r}\left(\lambda r \frac{\partial T_g(r,z)}{\partial r}\right) + \frac{\partial}{\partial z}\left(\lambda \frac{\partial T_g(r,z)}{\partial z}\right) = -(q_f'''(r,z) - h\alpha(T_g(r,z) - T_c(r,z))). \tag{3-13}$$

3-1-3 Numerical appromation of $T_g(r,z)$

In this section Equation 3-13 will be numerically approximated for $T_g(r,z)$ using the discontinous Galerkin finite volume method. To find a numerical approximation of this differential equation, the region Ω_{rz} over which this equation holds, is subdivided into discretized cells. For example, in 1D, the interval could be subdivided in subintervals with length Δx_k, $k = 1, ..., N$, where Δx_k is bound by nodal points (x_{k-1}, x_k), see Figure 3-1.

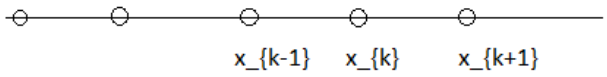

Figure 3-1: Example of a discretized grid. [9]

In order to determine the temperature at x_k, one would set up a control volume around it, the boundaries of this control volume would be $(x^k_{k-\frac{1}{2}}, x^k_{k+\frac{1}{2}})$.

The same principle applies in 2D, Equation 3-13 is discretized into cells with equal length and height and a constant discretized temperature $T^{k,l}$. For each of these nodal points, a control volume is set up to help determine the coefficients $T^{k,l}$. An example of a general control volume is shown in Figure 3-2. There is a node visible at the center C with a discretized temperature $T^{k,l}$, which will be denoted as T_c from now on. The surrounding nodes are on the east (E, $T^{k+1,l}$), west (W, $T^{k-1,l}$), north (N, $T^{k,l+1}$) and south (S, $T^{k,l-1}$) points. The control volume is given by the lowercase letters. This notation will be subsequently followed in the thesis. [9]

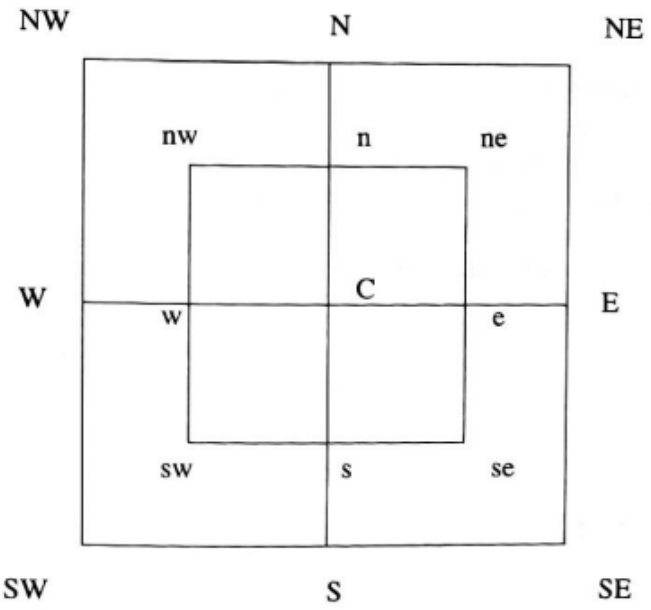

Figure 3-2: Example of a general control volume. There is a node at the center C with a discretized temperature $T^{k,l}$, which will be denoted as T_c from now on. The surrounding nodes are on the east (E), west (W), north (N) and south (S) points. The control volume is given by the lowercase letters. This notation will be followed in the thesis. [9]

In order to approximate a numerical solution for these temperatures $T_j^{k,l}$, the zeroth order discontinuous Galerkin (DG) method is employed. The DG method is a numerical method for solving differential equations. In the DG method, $T(r,z)$ will be approximated using a sum of J polynomials, which are called basis functions, $h_j^{k,l}$ for $j = 1, 2, ..., J$, multiplied by the coefficients $T_j^{k,l}$. In this thesis, j = 1, therefore the summation reduces to a single term. $T(r,z)$ can then be approximated by partitioning the two dimensional domain in NxN elements $\mathrm{e}_{k,l}$. Here $k = 1, 2, ..., N$ and $l = 1, 2, ..., N$. We then get

$$T_g(r,z) \approx u = \sum_{k=1}^{N}\sum_{l=1}^{N} T_j^{k,l} h_j^{k,l}(r,z). \tag{3-14}$$

Here we introduced a temperary variable u. To find the coefficients $T_j^{k,l}$, the DG method requires that the original differential equation is satisfied by the numerical approximation multiplied by some test function $h_j^{k,l}$ integrated over our discretized domain [25]. This cannot be satisfied on the entire domain Ω_{rz}, and therefore a weak approximation is used. Mathematically speaking, Equation 3-13 would be integrated as

$$-\int_{e_{k,l}} \frac{1}{r}\frac{\partial}{\partial r}\left(r\frac{\partial u}{\partial r}\right) h_m^k(r,z) + \frac{\partial}{\partial z}\left(\frac{\partial u}{\partial z}\right) h_m^k(r,z)\Omega_{rz} = \frac{1}{\lambda}\int_{e_{k,l}} q'''_{total}(r,z) h_m^k(r,z)\Omega_{rz}. \tag{3-15}$$

Due to time and complexity constraints, both $h_{i,j}^k(r,z)$ and $h_m^k(r,z)$ are set equal to 1 in this thesis, $h^k = 1$, on the edges of the discretized cells. Therefore, Equation 3-15 simplifies to

$$-\int_{e_{k,l}} \frac{1}{r}\frac{\partial}{\partial r}\left(r\frac{\partial u}{\partial r}\right) + \frac{\partial}{\partial z}\left(\frac{\partial u}{\partial z}\right)\Omega_{rz} = \frac{1}{\lambda}\int_{e_{k,l}} q'''_{total}(r,z)\Omega_{rz}. \tag{3-16}$$

This integral can now be solved for each element in the discretized grid. By realizing that $\Omega_{rz} = rdrdz$ and rewriting the left hand side as a dot product, it is found that

$$-\int_{e_{k,l}} \left(\frac{\partial}{\partial r}, \frac{\partial}{\partial z}\right) \cdot \left(r\frac{\partial u}{\partial r}, r\frac{\partial u}{\partial z}\right) drdz = \frac{1}{\lambda}\int_{e_{k,l}} q'''_{total}(r,z) r drdz. \tag{3-17}$$

It follows that the left hand term consists of the divergence operator multiplied by some vector field, therefore, the Divergence theorem can be applied, transforming the surface integral over the discretized cell in a line integral over the closed piecewise continuous boundaries of the cell:

$$-\int_{e_{k,l}} \left(\frac{\partial}{\partial r}, \frac{\partial}{\partial z}\right) \cdot \left(r\frac{\partial u}{\partial r}, r\frac{\partial u}{\partial z}\right) drdz = -\oint_{e_{k,l}} (n_r, n_z) \cdot \left(r\frac{\partial u}{\partial r}, r\frac{\partial u}{\partial z}\right) d\Gamma. \tag{3-18}$$

The equation now contains a line integral over the boundaries of the control volume on the left hand side, and a volume integral over $q'''_{total}(r,z)$ on the right hand side. To discretize the right hand side integral, dr is replaced by Δr, the width of the control volume, and dz is replaced by Δz, the height of the control volume. For the left hand side, dz is replaced by Δz, but the function contains an r, so integration over dr for the boundary segments is still required.

The center C has coordinates (r_C, z_C), and the volume integral is then approximated by the average value of $q'''_{total}(r, z)$ on these coordinates [9]:

$$\frac{1}{\lambda}\int_{e_{k,l}} q'''_{total}(r,z)rdrdz \approx \frac{q'''_{total}(r_C, z_C)}{\lambda} r_C \Delta z \Delta r. \tag{3-19}$$

For the left hand term, the boundary integral is obtained by the sum of the approximations over all boundary segments. [9] We evaluate the sum by going counterclockwise around the boundary. Substituting these approximations in Equation 3-17 gives us

$$r_w \frac{T_{g,W} - T_{g,C}}{\Delta r}\Delta z + r_e \frac{T_{g,E} - T_{g,C}}{\Delta r}\Delta z + r_C \frac{T_{g,N} - T_{g,C}}{\Delta z}\Delta r + r_C \frac{T_{g,C} - T_{g,C}}{\Delta z}\Delta r = \frac{q'''_{total}(r_C, z_C)}{\lambda} r_C \Delta z \Delta r, \tag{3-20}$$

where $q'''_{total}(r_C, z_C)$ is now discretized and given by

$$q'''_{total}(r_C, z_C) = q'''_f(r_C, z_C) - h\alpha(T_{g,C}(r_C, z_C) - T_{c,C}(r_C, z_C)). \tag{3-21}$$

Lastly, it is needed to determine the boundary conditions of the discretized core in order to solve Equation 3-20. For the left hand side of the core, the temperature is highest due to the symmetry of the problem, therefore $\frac{\partial T}{\partial r} = 0$. The other boundaries are chosen to be Neumann boundary conditions. This implies that the remaining three boundaries are isolated and therefore we have $\frac{\partial T}{\partial r} = 0$ and $\frac{\partial T}{\partial z} = 0$ for the z-axis boundary and r-axis boundaries respectively. The four corner cells of the system each have two boundary conditions imposed upon them. In chapter 4 the equations obtained will be used to determine the temperature distributions for the components mentioned and these distributions will be used to research the effect they have on k_{eff}.

3-1-4 Methodology

Equations 3-6, 3-20 and 3-21 are used to determine a temperature profile for the reactor core. Equation 3-6 can be solved with the use of a computer, the results of which are displayed in chapter 4. For the numerical approximation of the differential equation derived in the previous section, a small algorithm is written in Python.

The algorithm initially assumes a set temperature T_g for the discretized cells in the reactor core. It then iteratively updates T_g by applying Equation 3-20 $1 \cdot 10^4$ times. The corner cells are first calculated, followed by the boundary cells and finally the remaining cells in the center of the reactor core. Figure 3-3 displays a schematic overview of the algorithm used to calculate the temperatures. The output contains the graphite temperatures for the nodes of the discretized cells. The discretized cells are laid out in a structured mesh of squares, and the structured mesh contains 100x100 cells.

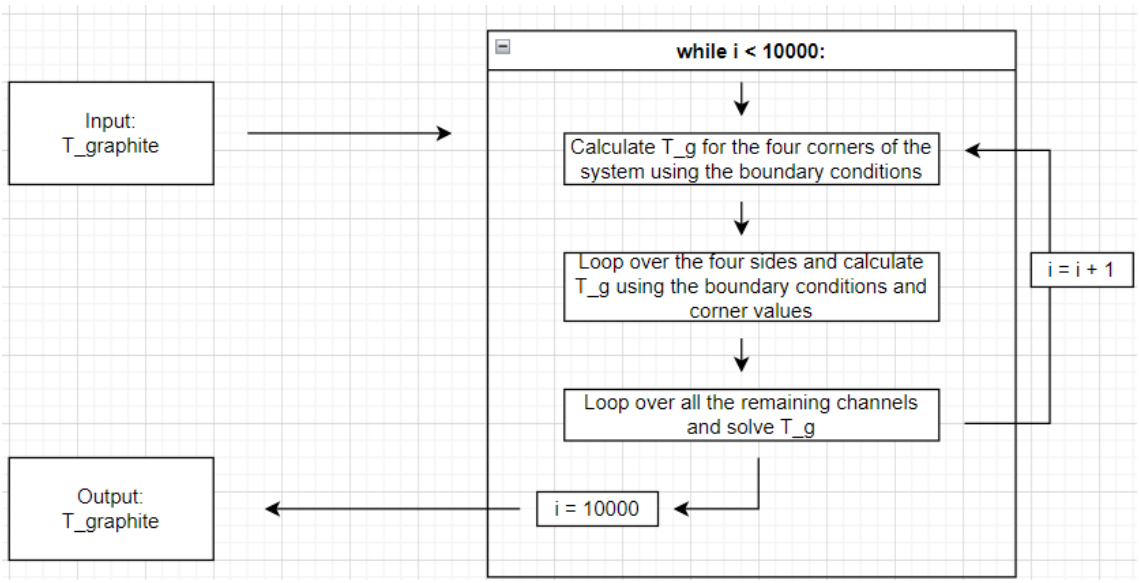

Figure 3-3: Schematic overview of the algorithm applied to calculate the graphite temperatures throughout the core for each of the nodes of the discretized cells.

Chapter 4

Results & Discussion

This section will cover and discuss the numerical results obtained in this research. First, the temperature distribution of a TRISO-particle has been determined using Equations 11 and 13; and Table 2. These values are used in combination with the assumption that $T_6 = 800K$ at $r = R_6$ to determine the core temperature. The initial calculation gives a temperature of $T_0 = 802.17K$ at $r = 0$, implying a temperature difference of $\Delta T = 2.17K$ between the core and outer shell of the TRISO-particle. Figure 4-1 shows the temperature as a function of radial distance from the core, as well as showing the cell boundaries as dashed lines.

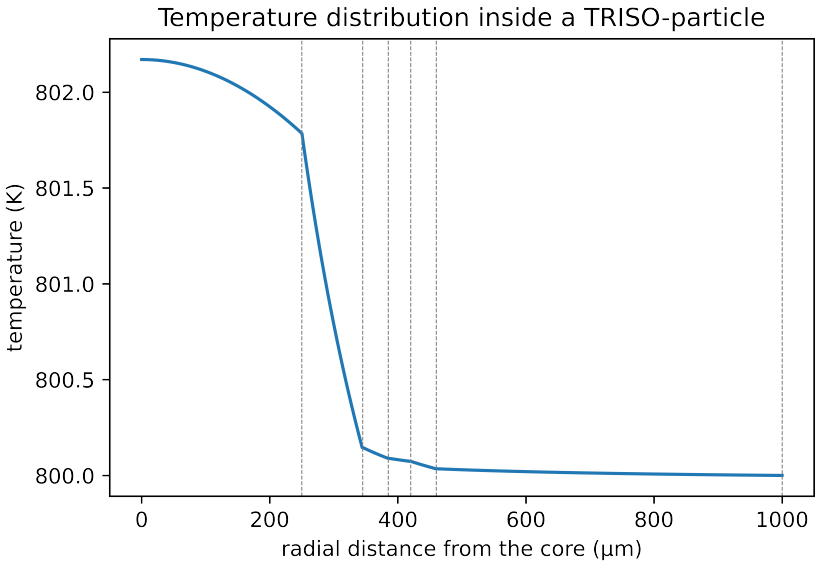

Figure 4-1: The temperature inside a TRISO-particle as a function of its radius. The dashed vertical lines represent a transition into another material. The radius of the triso particle is 460μm. The remaining material is the graphite moderator.

The dashed vertical lines represent a transition from layer to layer, with the outer layer of the TRISO-particle being at 460 μm. The remaining material used is the moderator graphite.

Noticeable is how the temperature decreases as $\propto r^2$ for the kernel of the TRISO-particle, but is inversely proportional with r in the outer layers. This directly follows from Equations 2.9 and 2.11. It is also clear that the largest temperature difference occurs in the buffer material, as this has the lowest thermal conductivity of the materials. The temperature distribution over the TRISO-particle will result in a change of k_{eff} over the particle. This will be quantified and expanded upon once the FTC is determined, later on in the chapter.

The temperature distribution was calculated using a thermal conductivity of 0.25 [W/cmK] for graphite. This value is taken from Liu [2]. The same calculation could be done by assuming a worse thermal conductivity for graphite, in order to ensure that even in the worst case it is known what the implications are for k_{eff}. The value we then take for $\lambda_g = 0.10$ [W/cmK]. We find that the maximum temperature is $T_{max} = 802.22K$ at $r = 0$. This temperature increase of $\Delta T = 0.04K$ compared to T_0 for $\lambda_g = 0.25$ [W/cmK] is small and, as will be seen later on, barely influences k_{eff}. Furthermore, the volumetric power density of a TRISO-particle was calculated assuming a packing fraction $\phi = 0.3$ of TRISO's in a fuel pin. However, as seen in Figure 2-7, this slightly varies throughout a fuel pin and greatly increases at the inner surface of the fuel pin. The actual packing fraction of the fuel pin could slightly differ, resulting in a increased or decreased maximum temperature for a TRISO-particle.

As mentioned in chapter 2, the distribution for the fission power in Figure 2-7 has been normalized. This has been done by requiring that the sum of all volumetric power densities multiplied by their respective volumes (of the 'rings') be equal to the power output of the U-battery® divided by the total number of fuel pins inside the U-battery®. The resulting volumetric power densities and packing fractions have been used to determine the temperature distribution inside a fuel pin using Equation 2.24. The packing fraction is displayed in Figure 4-2 and the temperature distibution is displayed in Figure 4-3. An important assumption we made here, is that the fuel pin in question is assumed to be in the center of the core. Due to this assumption, we assume that the volumetric power density of a TRISO particle is twice as high as it would be at the edge, which ties back to the assumed cosine distributions for q_f'''. This results in a temperature distribution twice as large as it would be for a fuel pin at the edge of the reactor core.

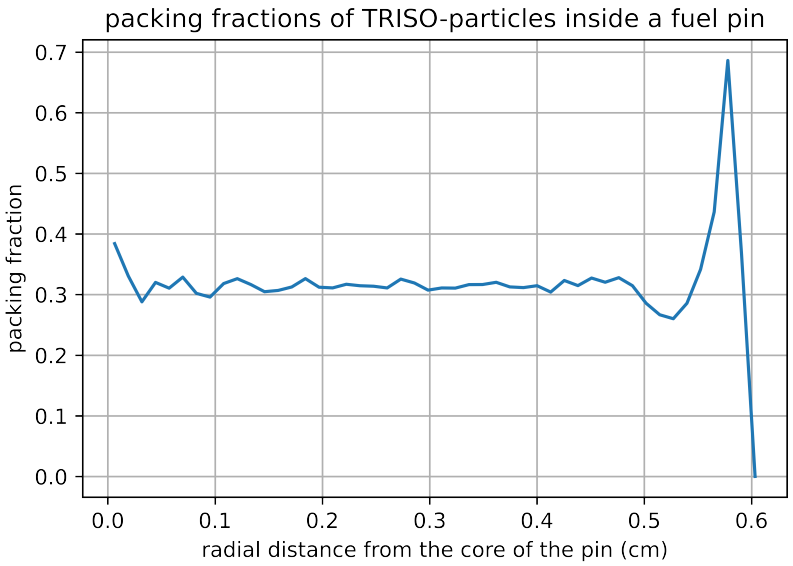

Figure 4-2: The packing fraction inside a fuel pin as a function of its radius. Notice the slight dip and the spike around $r = 0.6$cm [8].

Figure 4-2 shows that the packing fraction of TRISO's in a fuel pin hovers around 0.3 for the largest part of the pin. However, a slight dip and large peak are noted near the end of the plot. This could be explained due to the fact that the TRISO's potentially form a structured lattice at the inner surface of the fuel pin, increasing the packing fraction in that region. This has been noted before in Helmreich [26].

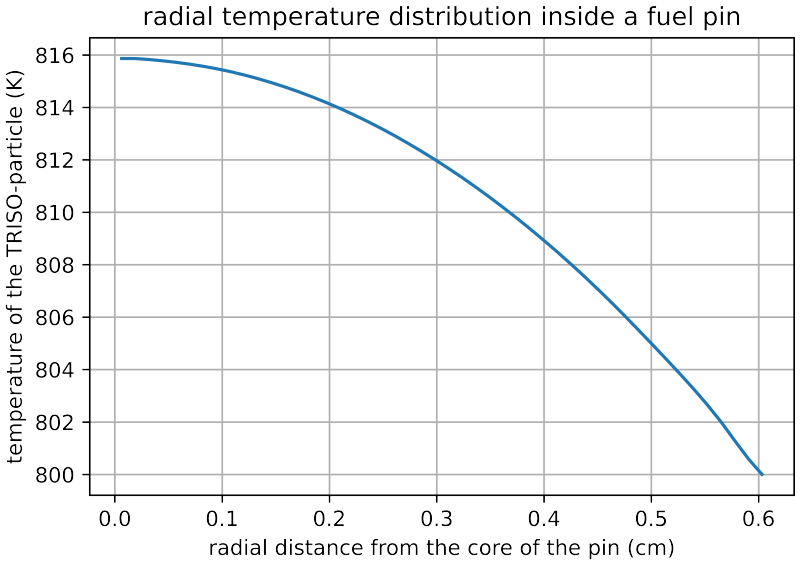

Figure 4-3: The temperature inside a fuel pin as a function of its radius. The temperature at the outer shell is set to $T = 800K$. The peak temperature is $T_{max} = 815.86K$.

Figure 4-3 displays the calculated temperature distribution of a fuel pin. The temperature difference between the outer shell and the core is $\Delta T = 15.86K$. Due to the packing fraction, and thus $\lambda_{e,i}$, remaining near constant, there are no large discrepancies in the continuity of the plot, as opposed to what has been seen in Figure 4-1. Noticeable is that at $r \approx 0.57$cm, the temperature has a slight kink. This is explained due to the sudden increase of the packing fraction, which slightly decreases $\lambda_{e,i}$, thus causing a slightly larger increase in temperature.

The assumption that the fuel pin is in the center of the core, where the power density is largest according to the approximated distribution, means that the maximum temperature differences should be lower for the other pins in the reactor core. This implies that, on average, k_{eff} will have a smaller decrease between the surface temperature and maximum temperature of the fuel pin. This thesis will continue working with the temperature distribution of the center fuel pin to provide an estimate for the maximum change in k_{eff} that could occur in a fuel pin.

Important for the U-battery® is to minimize local temperature changes in order to ensure a stable k_{eff}. We can do this by varying the packing fraction of TRISO-particles. One of these variations is when all the TRISO-particles are located past $r > R/2$, and there are no TRISO's for $r < R/2$. The temperature distribution that then arises is displayed in Figure 4-4 and the corresponding packing fraction is displayed in Figure 4-5.

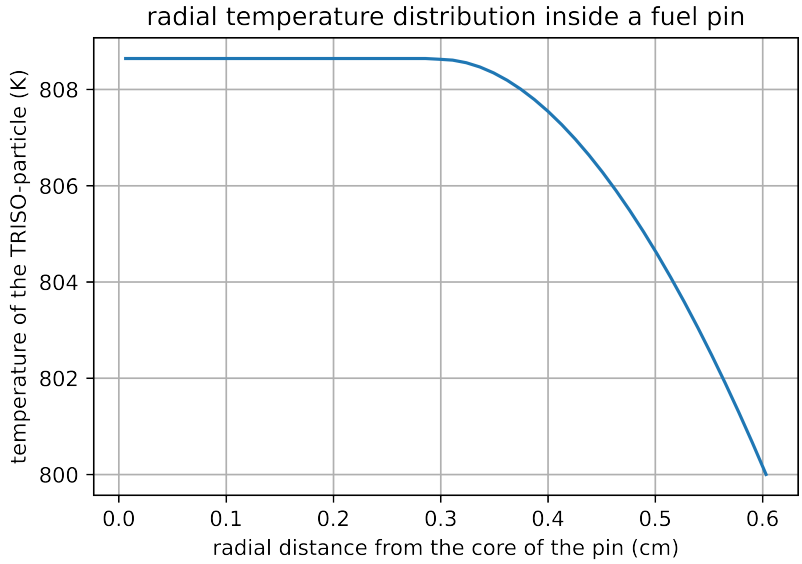

Figure 4-4: The temperature inside a fuel pin as a function of its radius assuming packing fraction where all the TRISO-particles are located past $r > R/2$, and there are no TRISO's for $r < R/2$.. The temperature at the outer shell is set to $T = 800K$. The peak temperature is $T_{max} = 808.64K$.

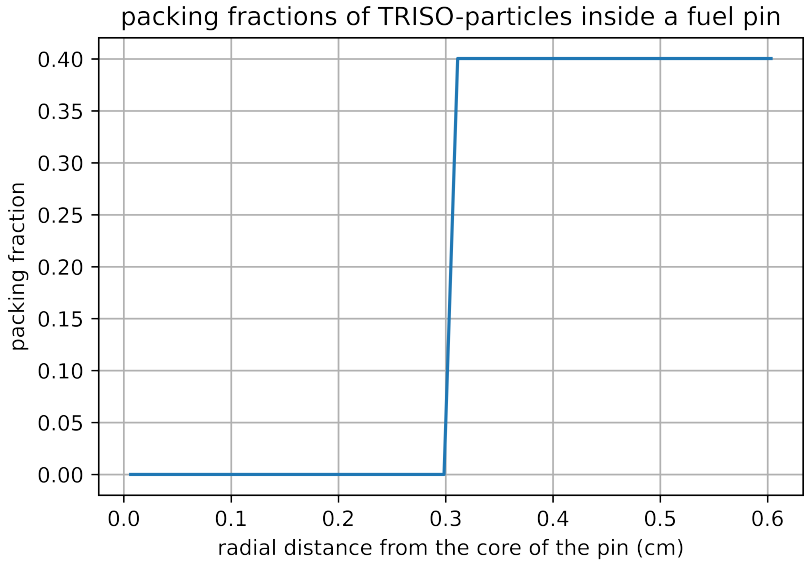

Figure 4-5: One of the assumed variations of the packing fraction inside a fuel pin as a function of its radius.

A noticeable result that arises is that the maximum temperature in the fuel pin using the packing fraction in Figure 4-4 is $T_{max} = 808.64K$, almost half of the original maximum temperature. It follows that, if possible, the TRISO's could be ordered differently, resulting in a different packing fraction and ensuring a lower maximum temperature and thus less changes in k_{eff}.

Having determined the temperature distribution in the fuel pin, the effect of changes in the fuel (and moderator) temperature on the reactivity can be researched. First, the fuel pin is assumed to have a uniform temperature distribution of $800K$. k_{eff} is then calculated in Serpent using the geometry displayed in Figure 2-8. Afterwards, the calculated temperature distribution is applied in Serpent and k_{eff} is calculated. Using these values the reactivity and FTC are calculated.

For the uniform temperature distribution, it is found that $k_{eff} = 1.41535 \pm 1{\cdot}10^{-5}$. For the calculated temperature distribution, $k_{eff} = 1.41455 \pm 1{\cdot}10^{-5}$. Therefore $\Delta k_{eff} = -80 \pm 1.4$ pcm. Equation 2.2 can then be used to calculate the FTC for the fuel pin. However, $\frac{\partial k_{eff}}{\partial T_f}$ is linearly approximated around $T = 800K$, as the exact relation between k_{eff} and T_f is not known and approximated using Monte Carlo methods by Serpent. The temperature difference in T_f is taken as the difference between the temperature at the outer edge, which is $800K$, and the temperature of the core of a TRISO particle in the center of the pin, which is $\approx 818K$. Plugging this in, $\alpha_f = \frac{1}{1.41455^2} \frac{-8.0{\cdot}10^{-4}}{18} \approx -2.22$ pcm/K. The literature shows that an average FTC of reactivity for low enriched uranium (LEU), which is being used in the U-battery®) is -2.15 pcm/K [27]. The found value agrees well with the literature. For future research, the FTC could be decided by assuming an average temperature distribution over the fuel pin, instead of the calculated temperature distribution. This could further simplify the calculations for a future model of the U-battery®.

For the TRISO-particle, with a maximum temperature difference of $\Delta T = 2.18K$, we find that the absolute difference in k_{eff} between the outer surface and the core is 4.84 pcm. For a fuel pin in the center of the core, with a maximum temperature difference of $\Delta T = 15.86K$, we find that the absolute difference in k_{eff} between the outer surface and the core is 35.20 pcm. This difference can likely be neglected in a future model of the U-battery®, as values of k_{eff} for the entire U-battery® have an uncertainty in the order of 100 pcm according to literature [28]. Therefore the temperature differences within a TRISO-particle and fuel pin can likely be neglected, especially as the fuel pin is a center fuel pin, meaning that all other fuel pins will have a lower difference in k_{eff}.

Lastly, the temperature distribution of the graphite in the core is determined. For this, the coolant temperature T_c has first been calculated. The results are displayed in Figure 4-6.

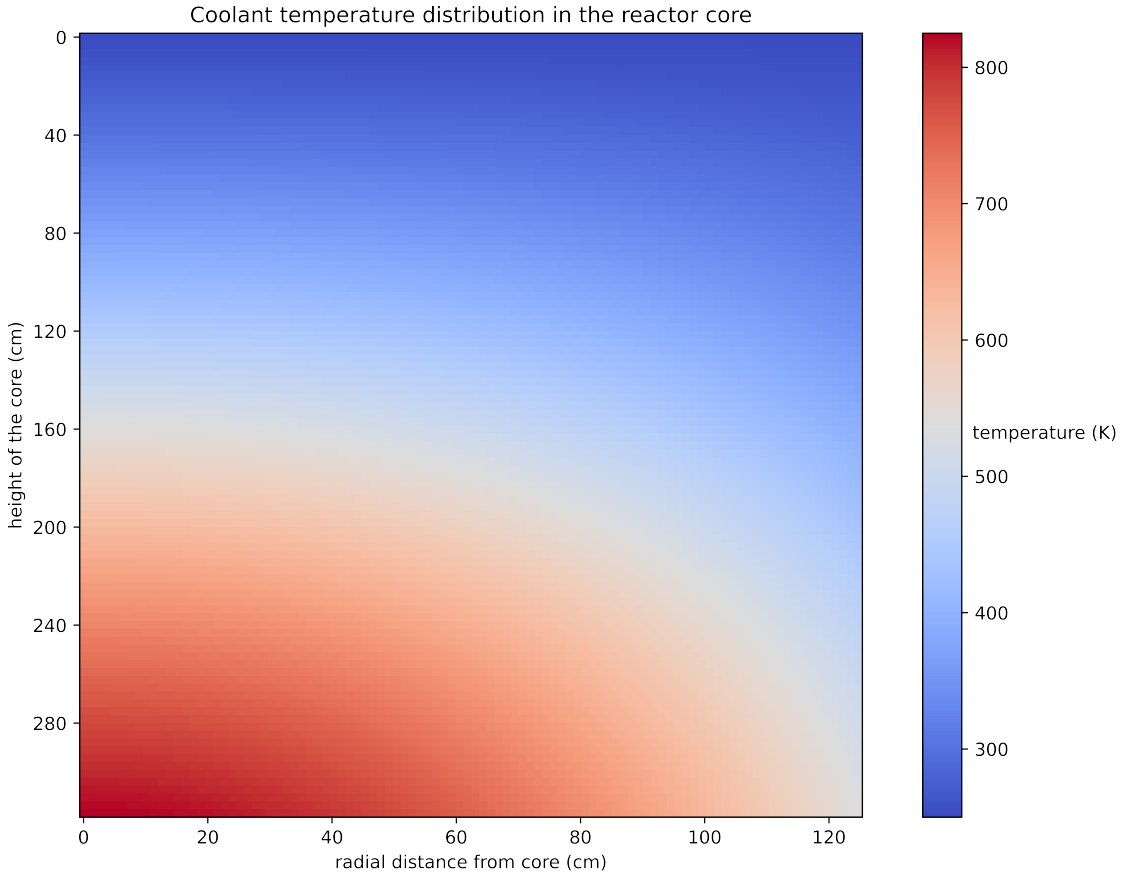

Figure 4-6: The temperature distribution of T_c inside the reactor core. The coolant flows in at $z = 0$cm with $T_{in} = 523K$. The coolant flows downward in the z-direction. As the coolant flows downwards, the power received from the surrounding graphite varies by a cosine distribution, increasing the temperature more in the middle of the core and less towards $z = 320$cm

The coolant flows in at $z = 0$cm with $T_{in} = 523K$, and increases in temperature as it flows downward. The maximum temperature for T_c at $z = 0$cm is $T_{max} = 1098K$. On average, T_c increases by $\Delta T \approx 475K$ from $z = 0$cm to $z = 320$cm. Furthermore, the increase in temperature is higher closer to the core, as the power density increases closer to the core as well. The temperature ranges from $T = 1098K$ at $r = 0$cm to $T = 810.5K$ at $r = 126$cm at $z = 320cm$. This follows directly from equations 3.1 and 3.6. Finally, a numerical approximation of the temperature distribution inside the reactor core of the U-battery® is given in Figure 4-7.

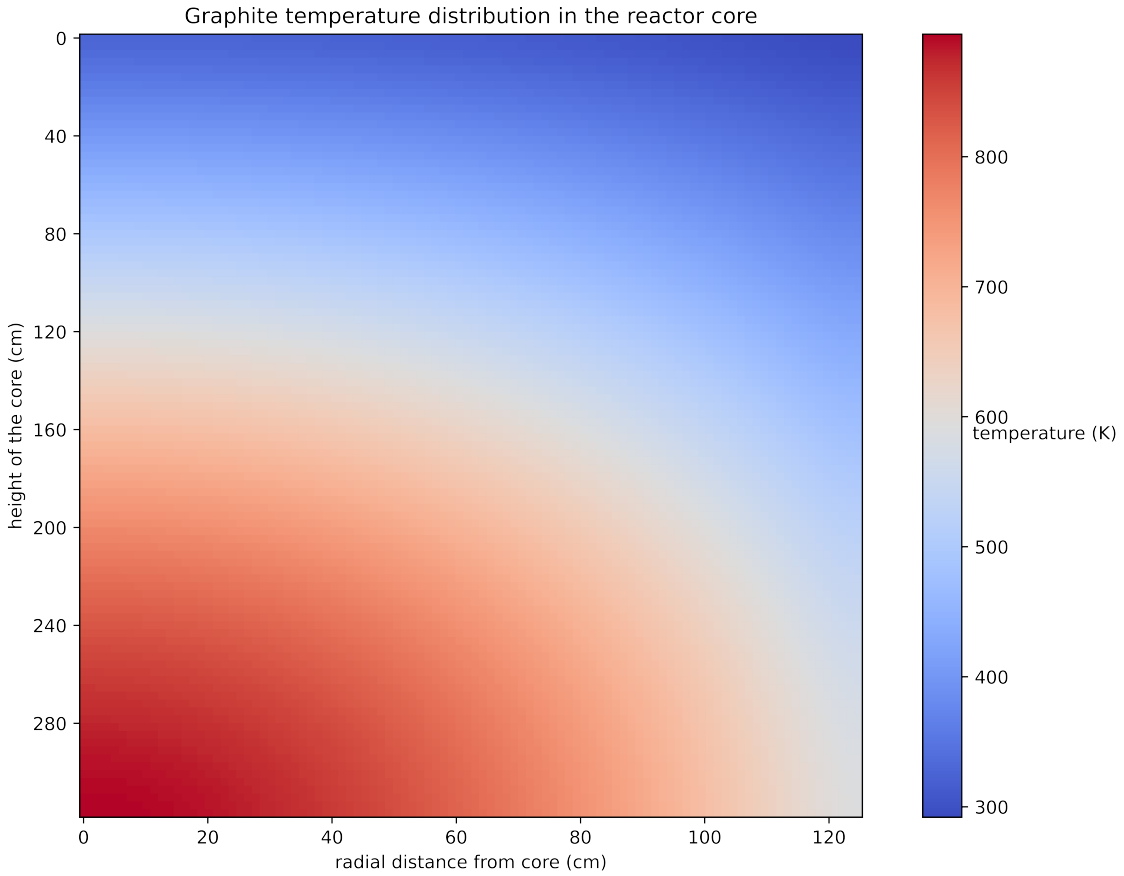

Figure 4-7: The temperature distribution of T_g inside the reactor core. T_g is lowest at $z = 0$ as the coolant is coldest there. T_g increases as more energy is transferred to the coolant, causing the coolant to increase in temperature and cool less the further it travels as the cooling capabilities are dependent on the temperature difference between the coolant and moderator.

Figure 4-7 displays the temperature distribution of T_g. The temperature ranges from $T = 600$K to $T = 1173$K at $r = 0$cm and from $T = 564$K to $T = 866$K at $r = R$. T_g is higher as r approaches 0. This follows directly from the symmetry of the geometry of the reactor core: the model assumes a homogeneous cylinder, and therefore the highest temperature occurs at $r = 0$cm. This can also be derived from Equation 3.1 for the volumetric power density q'''_f. q'''_f is highest for $r = 0$cm and $z = 160$cm. The heat map in Figure 4-7 is in agreement and shows the strongest increase in temperature for these coordinates. This is more clearly shown by plotting T_g for $r = 0$cm as a function of z, as shown in Figure 4-8.

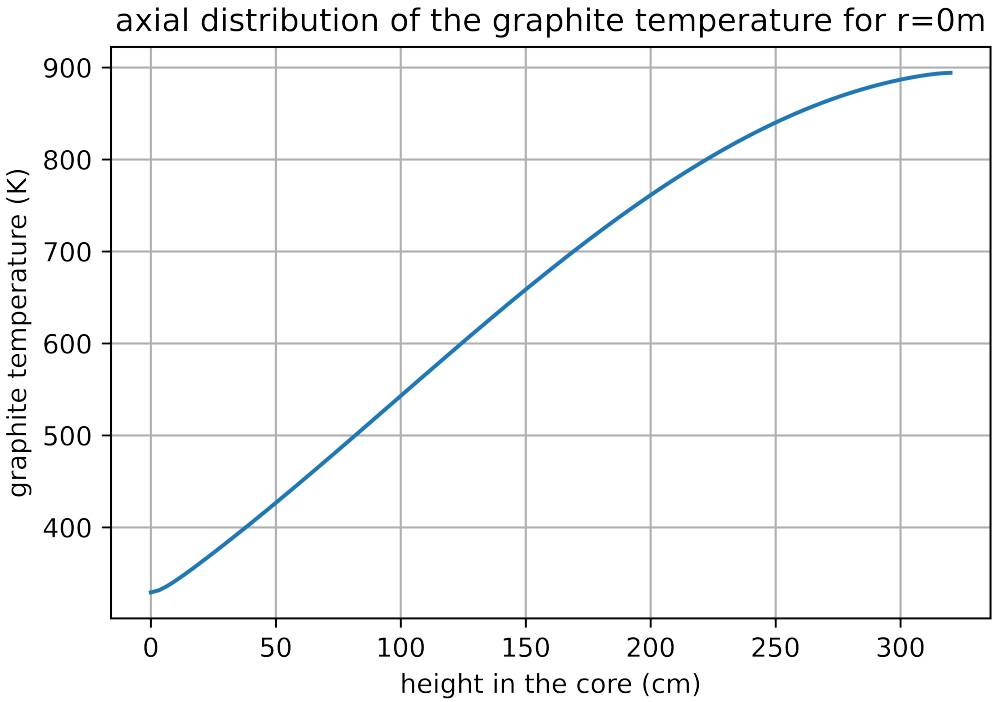

Figure 4-8: The temperature distribution of T_g for $r = 0$m as a function of z. Notice that the largest slope for the temperature occurs when $q_f^{'''}$ is largest.

Figure 4-8 also shows that the boundary conditions are correctly applied, as $\frac{\partial T_g(r,z)}{\partial z} = 0$ at $z = 0$cm and $z = 320$cm. Figure 4-9 shows that the same behaviour is seen for the radial distribution, where $\frac{\partial T_g(r,z)}{\partial r} = 0$ at $r = 0$cm and $r = 126$cm. This is displayed for $z = 0$cm and $z = 320$cm.

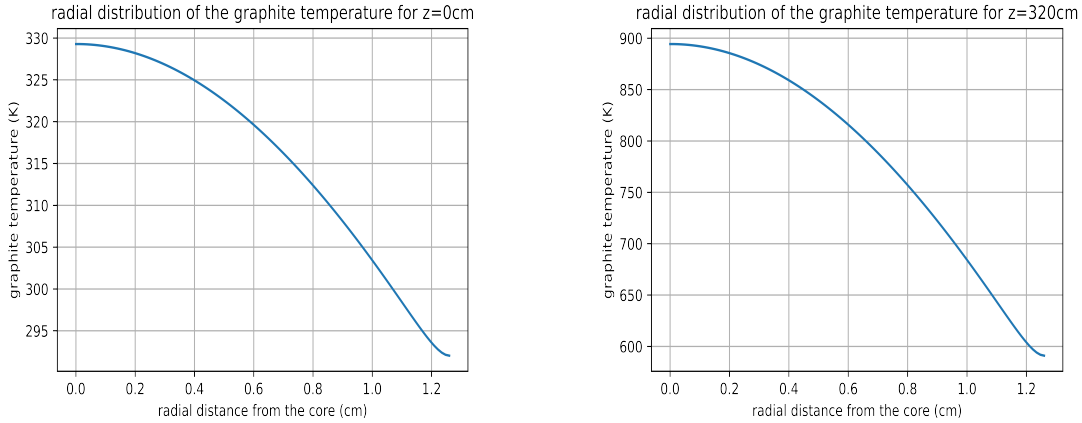

(a) The temperature distribution of T_g for $z = 0$cm as a function of r.

(b) The temperature distribution of T_g for $z = 320$cm as a function of r.

Figure 4-9: The temperature distribution of T_g for different values of z as a function of r. Notice that $\frac{\partial T_g(r,z)}{\partial r} = 0$ at $r = 0$ cm and $r = 126$cm.

The radial temperature distribution only has a $\Delta T \approx 30K$ between the $r = 0$cm and $r = 126$cm at $z = 0$cm, but the difference in temperature increases to $\Delta T \approx 300K$ at $z = 320$cm. This large difference in temperature could be explained by looking at the heatmap for T_c, where $\Delta T_c(r = 0cm) = 575K$, and $\Delta T_c(r = 126cm) = 277.50K$ as a function of z. Clearly, the temperature increase is twice as large in the center as it is at R_{max}. This ties back to the assumption made when determining q'''_f: the volumetric power density caused by fission follows a cosine distribution in both the r- and z-direction, where the boundaries of the core have a value of 0.5, and the center of the core has a maximum value of 1. Therefore, the coolant receives much more thermal energy at $r = 0$cm.

While the maximum temperature differences within a TRISO-particle and a center fuel pin do not significantly influence k_{eff}, the temperature distribution of the reactor core does. Over the core, k_{eff} largery varies due to the large temperature differences (because of the FTC) and furthermore the different temperatures also influence the FTC itself. k_{eff} decreases for temperatures higher than $800K$ (the temperature at which we calculated k_{eff}) and increases for temperatures lower than $800K$, this then influences the FTC, as it is directly dependent on k_{eff} per equation 2. It is therefore recommended to take into account the temperature distribution inside the reactor core, and divide the temperature distribution into rings with temperature differences. One potential rule of thumb to apply to the size of the rings is to have the temperature differences between the rings be in the order of the maximum temperature difference in the fuel pin, as we have seen that this does not exceed $\Delta k_{eff} = 100$pcm and likely will not for the given temperature distribution.

We assumed that the volumetric power density has a cosine distribution with the edges at 0.5 and the center at 1. In reality, however, this distribution is not symmetrical and is shifted toward the top of the core. Furthermore, we assumed that the graphite moderator does not conduct heat in the initial calculation of the coolant temperature, instead transferring all fission power to the coolant. In reality, however, the fission power can first be conducted

through the moderator, thus 'spreading out' the temperature more over the core. This could slightly decrease the differences in the given temperature distribution.

In future research the temperature distribution in the core could be modelled more accurately by taking into account all the cooling channels instead of homogenizing them. Furthermore, a more accurate distribution for the volumetric power density could be used. Lastly, the coolant temperature T_c can be more accurately determined by assuming that the graphite conductor does conduct heat in the initial calculation of T_c.

Chapter 5

Conclusion

In this research, the U-battery® is researched. The temperature distribution inside a TRISO-particle and a fuel pin is determined. This is done by deriving governing equations for the temperatures by applying Fourier's law and the heat equation. The found temperature distribution are determined in order to research the influence they have on the the neutron multiplication factor k_{eff}. Lastly, the temperature distribution of the coolant and the graphite moderator in the reactor core is determined by numerically approximating the heat equation using the discontinuous Galerkin finite volume method.

For a TRISO-particle, it is found that the maximum temperature difference between the core and the outer surface is $\Delta T = 2.17K$. For the fuel pin, the same assumption is applied and it is found that the maximum temperature difference between the core and the outer surface is $\Delta T = 15.86K$.

In the case of a uniform temperature distribution inside the fuel pin, it is found that $k_{eff} = 1.41535 \pm 1{\cdot}10^{-5}$. For the calculated temperature distribution, $k_{eff} = 1.41455 \pm 1{\cdot}10^{-5}$. The Fuel Temperature Coefficient (FTC) is then ≈ -2.22 [pcm/K]. The literature shows that an average FTC of reactivity for low enriched uranium (LEU), which is being used in the U-battery®, is -2.15 [pcm/K] [27]. The found value agrees well with the literature. Applying the FTC to the found maximum temperature differences for a TRISO-particle and a center fuel pin results in $\Delta k_{eff} = 4.84$pcm and $\Delta k_{eff} = 35.20$pcm respectively. These differences in k_{eff} are not significant and can therefore be neglected in a future model of the U-battery®.

For the temperature distribution of the reactor core, we find that the temperature of the coolant T_c flows in at $T_{in} = 523K$ and on average increases by $\Delta T \approx 475K$ over the height of the reactor. The graphite temperature T_g ranges from $T = 600$K to $T = 1173$K at $r = 0$cm and from $T = 564$K to $T = 866$K at $r = R$. On average, T_g increases by $\Delta T \approx 467K$ over the height of the reactor.

In conclusion, this thesis derived the temperature distributions for a TRISO-particle and a fuel pin, and used these distributions to determine the FTC. The FTC ≈ -2.22 [pcm/K]. This value does not result in a significant change of k_{eff} for a TRISO-particle and the fuel pins and can therefore the temperature distributions for these can be neglected in a future model of the U-battery®. Furthermore, an approximation of the temperature distribution inside the reactor core is derived and numerically approached. For this temperature distribution, the FTC does result in significant changes in k_{eff}, therefore it is recommended to take the temperature distribution of the reactor core into account in a future model of the U-battery®.

In future research the temperature distribution in the core could be modelled more accurately by taking into account all the cooling channels instead of homogenizing them. Furthermore, a more accurate distribution for the volumetric power density could be used. Lastly, the coolant temperature T_c can be more accurately determined by assuming that the graphite conductor does conduct heat in the initial calculation of T_c.

Bibliography

[1] Ming Ding, Jan Leen Kloosterman, Theo Kooijman, Rik Linssen, Tim Abram, Barry Marsden, Tony Wickham. *Design of a U-battery®*. 2011.

[2] Maolong Liu, Jared Thurgood, Youho Lee, Dasari V. Rao. *Development of a two-regime heat conduction model for TRISO-based nuclear fuels*. 2019.

[3] Nuclear magic numbers. https://chem.libretexts.org/@go/page/1483, 2020, September 22. Consulted on 06-02-2022.

[4] N. Soppera, M. Bossant, E. Dupont. *JANIS 4: An Improved Version of the NEA Java-based Nuclear Data Information System*. Nuclear Data Sheets, Volume 120, P.294-296., 2014.

[5] Doppler broadening – doppler effect. https://www.nuclear-power.com/glossary/doppler-broadening/, 2019. Consulted on 08-02-2022.

[6] H. Sekimoto. *Nuclear Reactor Theory*. COE-INES, Tokyo Institute of Technology., 2007.

[7] J. R. Lamarsh. *Introduction to Nuclear Reactor Theory*. 2nd ed., Addison-Wesley, Reading, MA, 1983.

[8] M. Van den Berg. personal communication, December 14, 2021.

[9] J. Van Kan, A. Segal, F. Vermolen. *Numerical Methods in Scientific Computing*. Delft Academic Press, second edition, 2014.

[10] H. Petersen. *The properties of helium: Density, specific heats, viscosity, and thermal conductivity at pressures from 1 to 100 bar and from room temperature to about 1800K*. Risø National Laboratory, 1970.

[11] https://www.climate.gov/news-features/understanding-climate/climate-change-global-temperature#:~:text=August%2012%2C%202021-,Highlights,land%20areas%20were%20record%20warm., 2021. Consulted on 26-01-2022.

[12] Ming Ding, Jan Leen Kloosterman. *Parametric Neutronics Design of a Small and Long-Life HTR.* 2010.

[13] https://www.u-battery.com/about, 2022. Consulted on 24-01-2022.

[14] https://www.energy.gov/ne/articles/triso-particles-most-robust-nuclear-fuel-earth, 2019. Consulted on 24-01-2022.

[15] P. Mills, R. Soto, G. Gibbs. *Next Generation Nuclear Plant Pre-conceptual Design Report.* Idaho National Laboratory (INL), 2007.

[16] W. M. Stacey. *Nuclear Reactor Physics.* John Wiley Sons, 2001.

[17] Y. Shimazu. *Molten Salt Reactors and Thorium Energy.* Elsevier Ltd. University of Fukui., 2007.

[18] Theodore L. Bergman, Adrienne S. Lavine, Frank P. Incropera. *Fundamentals of Heat and Mass Transfer.* John Wiley Sons, Incorporated, 7th edition edition, 2011.

[19] E. E. Gonzo. *Estimating correlations for the effective thermal conductivity of granular materials.* Chem. Eng. J. 90 (3) P. 299-302, 2002.

[20] Y.C. Chiew, E.D. Glandt. *The effect of structure on the conductivity of a dispersion.* Journal of Colloid and Interface Science 94 (1) P. 90-104, 1983.

[21] C. Folsom et al. *Experimental measurement and numerical modeling of the effective thermal conductivity of TRISO fuel compacts.* Journal of Nuclear Materials 458 P.198–205, 2015.

[22] R. Stainsby, A. Grief, M. Worsley, F. Dawson. *Investigation of local heat transfer phenomena in a pebble bed HTGR core.* AMEC Nuclear NR001/RP/002 R01, 2009.

[23] Theodore L. Bergman, Adrienne S. Lavine, Frank P. Incropera. *Fundamentals of Heat and Mass Transfer.* John Wiley Sons, Incorporated, 7th edition, 2011.

[24] Gilbert Melese and Robert Katz. *Thermal and Flow Design of HeliumCooled Reactors.* American Nuclear Society, 1984.

[25] D. Lathouwers. *Essentials of Discontinuous Galerkin Finite Element discretization for neutron transport.* 2014.

[26] G.W. Helmreich, et al. *New method for analysis of X-ray computed tomography scans of TRISO fuel forms.* Oak Ridge National Laboratory, Nuclear Engineering and Design 357 110418, 2020.

[27] Phan Thi Thuy Giang, Do Quang Binh. *Evaluation of the reactivity feedback coefficients of the Da Lat nuclear research reactor using highly enriched uranium fuels and low enriched uranium fuels.* Ho Chi Minh City University of Technology and Education, 2015.

[28] Ming Ding, Jan Leen Kloosterman. *Thermal-hydraulic design and transient evaluation of a small long-life HTR.* Nuclear Engineering and Design 255 (2013) P.347–358.